Geodinamica Acta

Geodinamica Acta 19/5 (2006) 301-321

Pressure-Temperature-time Evolution of Metamorphic Rocks from Naxos (Cyclades, Greece): Constraints from Thermobarometry and Rb/Sr dating

Stéphanie Duchêne [a]*, Rabha Aïssa[a], Olivier Vanderhaeghe[b]

[a] *Centre de Recherches Pétrographiques et Géochimiques UPR CNRS 2300, 15 rue Notre Dame des Pauvres, BP20, 54501 Vandœuvre-lès-Nancy, France*
[b] *Géologie et Gestion des Ressources Minérales et Energétiques UMR CNRS 7566, UHP Nancy 1, BP 239, 54506 Vandœuvre-lès-Nancy, France*

Received: 12/10/03, accepted: 02/02/05

Abstract

The Pressure-Temperature-time paths of metapelites sampled on an east-west transect across the structural dome of Naxos (Greece) have been reconstructed on the basis of new geothermobarometric data and Rb/Sr dating, as well as previously published data. One sample from an intermediate structural level records pressure and temperature conditions of 10 kbar, 500°C, corresponding to its exhumation in a high-pressure/low-temperature (HP/LT) setting. The corresponding Rb/Sr exhumation age is 29.3±1.3(2σ) Ma. Toward the center of the dome, metamorphic assemblages record an increase in peak-temperature and corresponding pressure (from 500 to 700°C, and from 5 to 8 kbar), in a medium-pressure/medium-temperature (MP/MT) metamorphic field gradient. Whole-rock, muscovite and biotite on two samples from deep structural levels define ages of 5.2 and 7.0 Ma, whereas garnets fall outside the isochrons and retain earlier less radiogenic signatures. Rb/Sr data on these two samples demonstrate open system behaviour coeval with, or subsequent to MP/MT metamorphism. The interpretation of the Pressure-Temperature-time paths indicates a time span of 15-20 Ma for dome formation. It also suggests that the HP/LT to MP/MT transition is due to i) heating of deeper parts of the dome through magma injection or ii) either homogeneous (75 %) or localized thinning during dome formation.

Keywords Naxos: / Metamorphic evolution/ Rb-Sr dating/Isotopic disequilibrium

1. Introduction

A common feature of orogenic belts (e.g. Caledonides, Variscan Belt) is the transition from a high pressure/low temperature (HP/LT) toward a medium pressure/medium temperature (MP/MT) thermal regime, coeval with the reduction of crustal thickness and topography [1, 2]. The geodynamic causes of this transition are not fully understood. The increase of thermal gradients during the orogeny (the so-called "thermal relaxation") is commonly viewed as a consequence of 1) crustal thickening which controls the heat supply through radioactive decay, and 2) mantle evolution, which controls the thermal fluxes at the base of the crust and the advection of heat via mafic magmas [2]. The relationship between crustal thinning, increase of the geothermal gradient, and partial melting of the crust is also a complex function of mutual dependence [3]. These relationships may be deciphered through field information on metamorphic, magmatic, and structural features in areas where this evolution

* Corresponding author.
Tel: +33 3 83 59 42 24 – Fax: +33 3 83 51 17 98
E-mail address: duchene@crpg.cnrs-nancy.fr

is recorded. The relative and absolute timing of these features must help investigate causual relationships between heat transfer, magmatism, and thickening/thining of the crust.

The island of Naxos is a well-studied example of a Metamorphic Core Complex in which HP/LT and MP/MT metamorphisms are superimposed. Metamorphic rocks are exposed in a structural dome cored by migmatites (Fig. 1). They are intruded by magmatic bodies, the most important of which is a granodioritic pluton that crop out on the western coast. Isolated sedimentary basins sample the erosion products of the crystalline rocks from the metamorphic dome and from the granodiorite [4]. Metamorphism affects a Mesozoic sedimentary sequence of shales and carbonates [5], mafic to ultramafic intercalations [6], and possibly an Hercynian basement in the core [7]. The metamorphic rocks record the evolution, recognized elsewhere in the Cyclades, from a high-pressure/low-temperature (HP/LT) regime, here represented by blueschist facies metasediments, toward a medium-pressure/medium-temperature (MP/MT) metamorphic regime, in greenschist to amphibolite facies conditions with associated partial melting.

It has been argued by Avigad and Garfunkel [8] and Gautier *et al*. [9] that the metamorphic rocks were exhumed along a detachment fault related to the extension of the Mediterranean domain during Miocene time [10-12]. Naxos therefore represents an ideal place to study the transition from a thickened toward a thinned crust, and the evolution from HP/LT and MP/MT metamorphic conditions. The point by point reconstruction of the coeval Pressure-Temperature-time (PTt) and structural evolutions of the metamorphic mid-crustal levels will help document and model the Naxos extensional history and decipher the interplay between the thermal state of the crust, partial melting, extension, and erosional processes. The present contribution discusses new thermobarometric and Rb-Sr geochronological data on metasedimentary rocks sampled at different structural levels and presents a reconstruction of the PTt paths for each of these structural levels on the basis of these new data and a review of the previously published data.

2. Previous PTt data on the metamorphic dome

2.1. Metamorphic evolution

Jansen and Schuiling [4] recognized that the dome shape structure of the island is paired with a concentric evolution of metamorphic features. They defined a series of metamorphic zones (Fig. 1) from the south-eastern part of the island (zone I) toward the migmatitic core (zone VI) on the basis of mineral isograds, and interpreted this zoning as a record of a metamorphic gradient increasing from 400°C, 5 kbar in the shallowest structural level toward 700°C, 7 kbar in the deepest. The present-day interpretation of the metamorphic zoning in Naxos considers the superposition of two distinct metamorphic events. A first HP/LT metamorphic stage, commonly referred to as M1 [4, 13], is recorded in south-east Naxos. The presence of a HP/LT metamorphism has been testified by the presence of glaucophane from zone I to zone III, as reported in Avigad [14]. Pressure and temperature estimates have been conducted by Jansen and Schuiling [4], Feenstra [15], Buick and Holland [13] and Avigad [14] (Table I). The discovery of jadeite-blueschists by Avigad [14] led him to the determination of minimum pressures of 12 kbar, for temperatures of 450-480°C, constrained by the presence of lawsonite and diaspore, and Fe/Mg garnet/clinopyroxene thermometry. A second metamorphic stage, referred to as M2, corresponds to the MP/MT metamorphic gradient [4, 13]. As already mentioned, on the basis of mineral isograds, Jansen and Schuiling [4] determined temperature conditions increasing from zone I toward zone VI. Their temperature estimates have been made assuming pressures of 5-7 kbar, inferred in particular from the presence of kyanite and estimations of water pressure in high-grade rocks. In zone I, a maximum temperature of 420°C had been inferred from the presence of diaspore, with the stability curve of Haas [16] for a pressure of 3 kbar. If diaspore instead belongs to the M1 paragenesis, the minimum pressure is 12 kbar, which converts to a maximum temperature of 500°C. According to Jansen and Schuiling [4], zone II extends from 420 to 500°C (appearance of biotite [17]), zone III from 500°C to 540-580°C (disappearance of chloritoid [18, 19]), zone IV from 540-580°C to 620-660°C (kyanite-sillimanite transition), zone V from 620-660°C to 660-690°C (onset of melting [20]), and zone VI above 690°C. Buick and Holland's [13] peak-PT estimates (6-7kbar, 670-700°C) are in accordance to those of Jansen and Schuiling [4]. Oxygen isotope thermometry performed on quartz-veins from zone IV (640±30°C) and V (635-690°C) by Putlitz *et al*. [21] agree with Jansen and Schuiling's earlier estimates [4].

Figure 1: Geological map of Naxos **(b)** and west-east cross section **(a)**. From [45, 46]. Samples location and metamorphic zones of Jansen and Schuiling [4] are reported.

2.2 Timing of the metamorphic evolution

Geochronological data have been obtained essentially from K/Ar, $^{40}Ar/^{39}Ar$, and U/Pb dating (Table II). The Eocene age of 45±5 Ma for M1 metamorphism was first recognized from Rb/Sr and K/Ar data on micas obtained by Andriessen *et al*. [22], and $^{40}Ar/^{39}Ar$ data obtained by Wijbrans and McDougall [23], and was confirmed by later U/Pb data on zircons [24, 25]. K/Ar and $^{40}Ar/^{39}Ar$ studies [22, 23, 26] revealed a zoning in the age pattern which mimics the metamorphic zoning defined by Jansen and Schuiling [4]. In the outermost part of the dome (zones I to III), the K/Ar and $^{40}Ar/^{39}Ar$ ages obtained on micas range from 25 to 50 Ma [22, 23, 26]. With the exception that the oldest ages are obtained on the south-eastern zone where HP/LT relicts are best preserved, there is no systematic zoning pattern from zone I toward zone III. These ages have been explained either by a

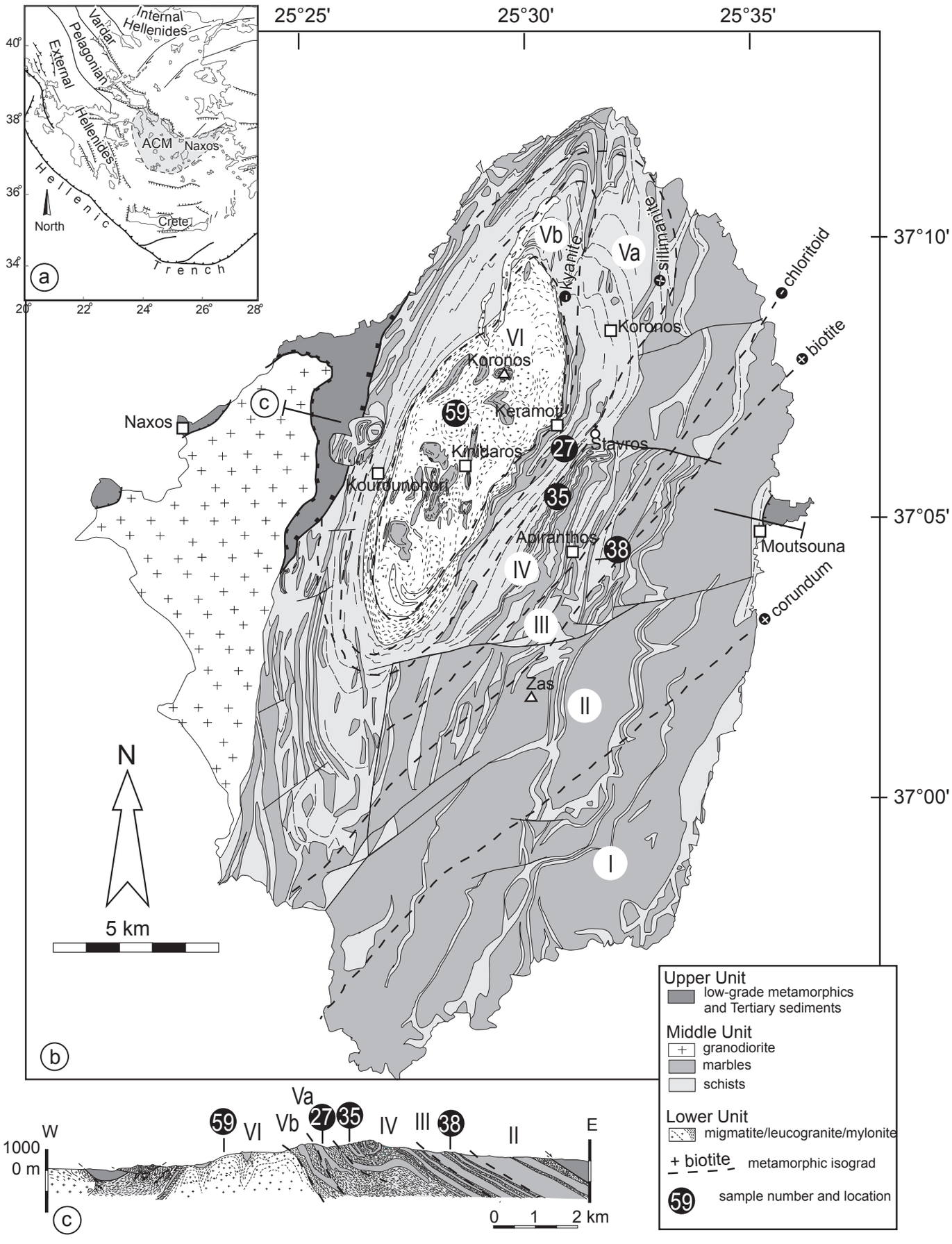

Table I - Pressure and Temperature estimates

Zone	Metamorphic stage	Authors	P kbars	T°C
I	M1	Buick and Holland [13]	> 9	250-450
		Feenstra [15]; Avigad [14]	>12	450-480
	M2	Jansen and Schuiling [4]	3-5	<420
II	M2	Jansen and Schuiling [4]	5-7	420-500
III	M2	Jansen and Schuiling [4]	5-7	500-580
IV	M2	Jansen and Schuiling [4]	5-7	540-660
V	M2	Jansen and Schuiling [4]	5-7	620-690
V	M2	Buick and Holland [13]	6-7	670-700
VI	M2	Jansen and Schuiling [4]	5-7	>690

rejuvenation of M1 mica ages during cooling, or by a mixing of micas of different (M1 and M2) generations [22, 23, 26, 27]. On this basis, an age of 20-25 Ma for the M2 greenschist facies retrogression has been proposed [22, 27]. However, the interpretation of $^{40}Ar/^{39}Ar$ plateau ages on hornblende led Wijbrans and McDougall to suggest an age of 15-20 Ma for peak M2 metamorphism [23]. In the inner metamorphic part of the dome (zones IV and V), the K/Ar and $^{40}Ar/^{39}Ar$ ages obtained on micas range from 10 Ma to 16.4 Ma [22, 23, 26, 27]. Lastly K/Ar and $^{40}Ar/^{39}Ar$ ages are the lowest (6-12 Ma) inside the migmatitic zone (zone VI). Because there is a tendency for ages to decrease from zone IV toward zone VI, John and Howard [28] suggested that these ages represented successive closure of the geochronological system throughout the exhumation process along the detachment zone, thereby providing a way to estimate the displacement rate along the detachment. Migmatization is probably best constrained by U/Pb SHRIMP ages on zircons from the migmatite obtained by Keay *et al*. [29], which extend from 16.8 to 20.7 Ma. This age span has been interpreted by the authors either as the persistence of partial melting conditions over ca. 5 Ma, or the existence of successive pulses of heating and subsequent partial melt production.

As a summary, a first group of ages, at 40-50 Ma, is thought to represent HP/LT metamorphism. Most of them are mica Rb/Sr, K/Ar, and $^{40}Ar/^{39}Ar$ ages which may be considered as cooling ages and thereby constitute minimum ages for the metamorphic event. Ages at ca. 20-23 Ma represent the youngest ages obtained in the outer part of the dome (zones I to III), and have been interpreted as early M2 muscovite re-crystallization [22, 27] or as mixing ages between micas of different generations [26]. The third group of ages (ca. 16-21 Ma) represents the main re-crystallization event related to M2 greenschist to amphibolite facies metamorphism, as well as partial melting (ca. 17-21 Ma) in the migmatic dome. Moreover, cooling ages obtained from Rb/Sr, K/Ar on amphiboles and micas are related to the exhumation of the dome at 10-15 Ma, and are coeval with late magmatic events and fluid circulation.

The above interpretations consider the superposition of two discrete metamorphic events in two distinct metamorphic gradients. However, geothermal gradients evolve continuously in time and space in orogenic environments, and we believe that a point-by-point reconstruction of the PTt path is essential. Accordingly, we have reconstructed the local PTt paths on few areas selected on an east-west traverse in zones III, IV, V and VI according to Jansen and Schuiling's terminology [4], on the basis of previously published data as well as the present petrological and Rb-Sr data.

3. Petrography

Major element analysis have been performed at the Service d'Analyse de l'Université Nancy I on a Cameca SX 50 electron microprobe with a beam current of 10 nA, and an acceleration voltage of 15 kV.

3.1. Sample NA 01 38, zone III

Sample NA 01 38 consists of quartz, white mica, garnet, albite and epidote, with small and late biotite (Fig. 2a). Garnet occur as isolated grains in the matrix or as inclusions in the plagioclase. They are almandine rich (X_{Fe}=0.61-0.77) and grossular rich (X_{Ca}=0.12 to 0.20). Garnets included in the plagioclase are small and euhedral (Fig. 2b), whereas outside the plagioclase (Fig. 2a), they are fragmented and rimed or partly replaced by a biotite/white mica/quartz association. However, the compositions are identical for both types of garnets (Fig. 4). They are characterized by slight (3 to 4 % in spessartine content) bell-shaped Mn zoning, indicating the preservation of growth zoning [30] (Fig. 5). Biotites are rich in Al^{VI} (X_{Al}^{VI}=16 %) and Ti (X_{Ti}^{VI} =5 %), and present Mg/(Mg+Fe) ratio in the range 0.44 to 0.51 (0.47 in average) (Table III). Two types of white micas can be recognized based on Si content (Fig. 6, Table III), thereby indicating a variation in the phengitic content. Muscovite occurs as small crystals (ca. 50 μm length) close to garnet and in association with biotite. Phengites with Si content of 3.4 to 3.5 cations per formula unit (calculated for 11 O) are by far the most abundant and consist of large (>300 μm) crystals deformed in the main foliation. They are also found as inclusions in plagioclase. A primary phengite/garnet/plagioclase/quartz paragenesis is therefore partly replaced by a muscovite/biotite/quartz association.

3.2. Sample NA 01 35, zone IV

Sample NA 01 35 consists of quartz, muscovite, biotite, garnet, kyanite, Fe-staurolite and tourmaline (Fig. 3a and b). Micas, kyanite and staurolite are aligned in the foliation.

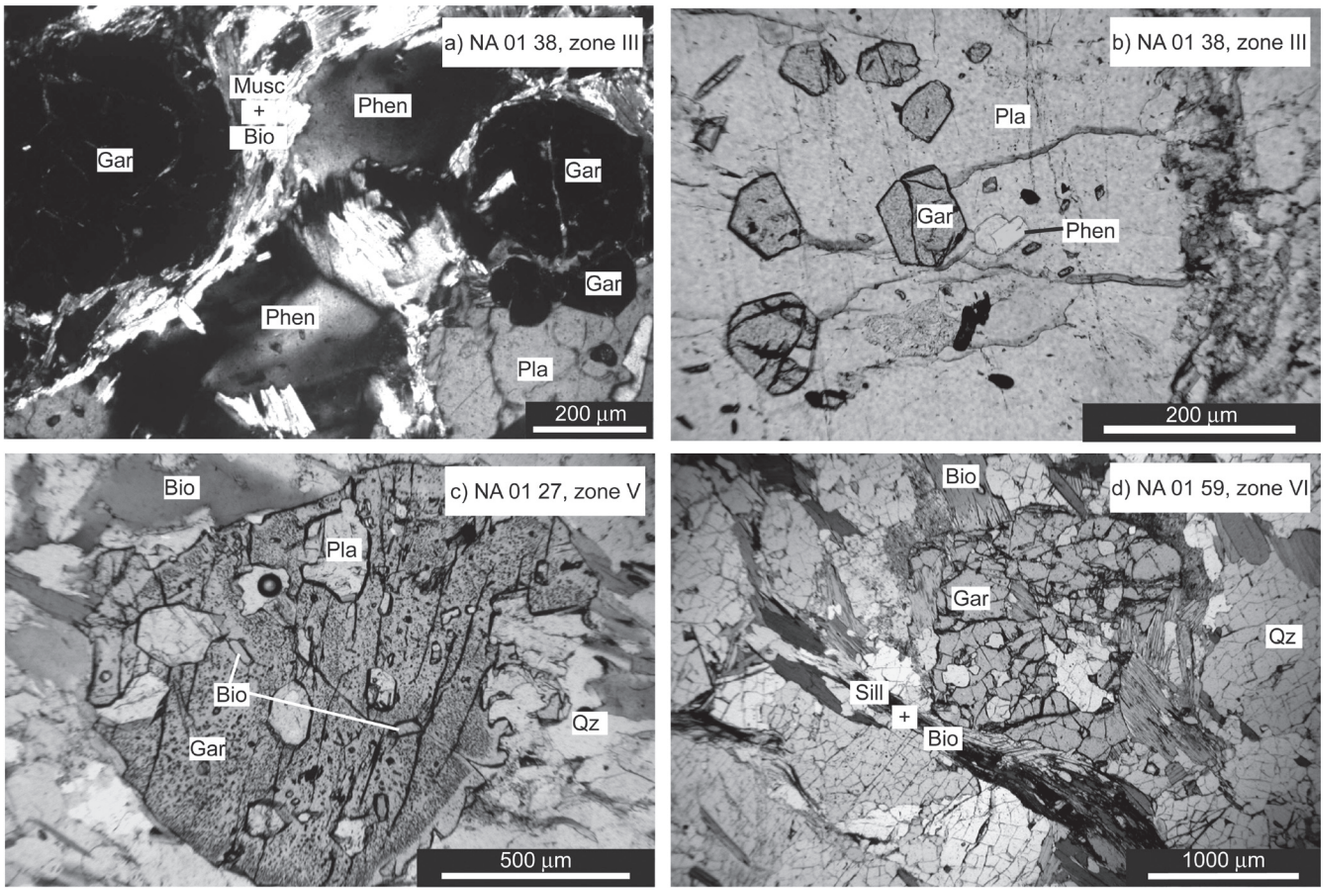

Figure 2: Photomicrographs of metamorphic rocks used for thermobarometry and geochronology
a) NA 01 38, zone III. Plagioclase is surrounded by large deformed phengite crystals. A fine-grained association of muscovite and biotite corresponds to the destabilization products of garnet crystals **b)** NA 01 38, zone III. Plagioclase contains euhedral garnet and phengite crystals **c)** NA 01 27, zone V. Plagioclase, quartz, and biotite inclusions in garnet. Note the presence of small graphite inclusions **d)** NA 01 59, zone VI. Garnet contains numerous inclusions of quartz and biotite.. Sillimanite fibres are localized at the end of biotite layers.

Staurolite appears in particular between garnet and kyanite (Fig. 3a) associated with biotite, or as rims around kyanite crystals (Fig. 3b). This suggests a reaction of appearance of staurolite such as the reaction kyanite+garnet =staurolite+quartz in KFMASH system. The white micas have a significant paragonite component (10-20 %) (Table III). Garnet grains exhibit a growth zoning also visible in SEM images (Fig. 3c and Fig. 5). Cores (light on SEM images) present flat concentration patterns and are Ca-poor (XCa ≈ 0.06) and Mn-rich (X_{Mn}≈0.9). They present rutile and ilmenite inclusions. A first rim (dark on SEM images) is characterised by bell-shaped Ca content (X_{Ca} reaches 0.14 at its maximum), and regular Mn-decrease (X_{Mn} ≈ 0.4 at garnet rims). The outermost part of the grains (30 μm) is characterized by antithetic Fe and Mg zoning patterns interpreted as retrogressive diffusion zoning [31, 32]. Biotites are rich in Al^{VI} (X_{Al}^{VI}=17 %) and Ti (X_{Ti}^{VI} =4 %), and present Mg/(Mg+Fe) ratio in the range 0.40 to 0.50 (0.46 in average). Variations in composition do not reflect internal zoning, but heterogeneity at the scale of the thin section.

3.3 Sample NA 01 27, zone V

Sample NA 01 27 consists of quartz, biotite, plagioclase, kyanite, rare garnet and rare muscovite (Fig. 2c). Faceted inclusions of plagioclase, biotite and quartz are present in the core of garnet crystals. There are many fine graphite inclusions in the garnet, disappearing at the rim. Plagioclase is albite rich (70 to 80 %). There is no obvious growth zoning in the garnets (Fig. 5), but a retrograde Fe-Mg zoning is observed at the contact with biotite (2 to 3 % of decrease in Mg/(Fe+Mg) ratio over a distance of 30-50 μm). Biotite presents no core/rim zoning. However, biotite compositions are heterogeneous at the scale of the thin section (Mg/(Fe+Mg) varies from 0.51 to 0.64, see Table III). Highest values are obtained in biotite inclusions inside garnet, which suggests that part of the heterogeneity in biotite composition is due to retrogressive exchange with garnet. This sample has not been selected for Rb/Sr dating, but provides the metamorphic P-T conditions in the core of the dome structurally just above the zone of partial melting.

Table II - Geochronological data and their interpretation by the authors

Zone	*Metamorphic stage*	*Authors*	*Method*	*Age (Ma)*
I	M1	Andriessen *et al*. [22]	Rb/Sr WR-Phen	48
	Cooling post-M1	Wijbrans and McDougall [26]	$^{40}Ar/^{39}Ar$ Phen	44 Ma
	Minimum for M1	Wijbrans and McDougall [23]	$^{40}Ar/^{39}Ar$ Phen	44.4-49.5
	M1+ Post-M1 resetting + Mixing	Andriessen *et al*. [22]	K/Ar Musc, Pg, Phen	40.2-48.3
	Post-M1 resetting	Wijbrans and McDougall [23]	K/Ar Phen, Pg	39.1-48.6
	Post-M1 resetting + Mixing	Wijbrans and McDougall [23]	K/Ar WM	38.5
	Post-M1 resetting + Mixing	Andriessen *et al*. [22]	K/Ar Phen, Chl	32.2-37.9
	Maximum for M2	Wijbrans and McDougall [23]	$^{40}Ar/^{39}Ar$ Phen	19.9-27
III	Post-M1 resetting + Mixing	Wijbrans and McDougall [26]	K/Ar WM	27.8
	M1-M2 transition	Andriessen *et al*. [22]	K/Ar Musc	19.1-29.3
	Mixing	Wijbrans and McDougall [23]	K/Ar Phen	27.8
	Mixing	Wijbrans and McDougall [23]	K/Ar Phen + Musc	25.6
	Mixing	Wijbrans and McDougall [23]	K/Ar Musc (± Phen)	20.7-21.1
	M2	Andriessen *et al*. [22]	K/Ar Hb	21.3
	Maximum estimate for M2	Wijbrans and McDougall [23]	$^{40}Ar/^{39}Ar$ Amph	19.8
	M2 Musc crystallization	Andriessen [27]	Rb/Sr WR-Musc	22.5
	M2 Musc crystallization	Andriessen [27]	K/Ar Musc	22.7
	Cooling post-M2 (ca.300°C)	Andriessen [27]	Rb/Sr WR-Bio	13.9
	Cooling post-M2 (ca.300°C)	Andriessen [27]	K/Ar Bio	14
	Cooling post-M2	Wijbrans and McDougall [23]	K/Ar Bio	12.5
IV	Cooling post-M2	Andriessen *et al*. [22]	K/Ar Hb	15.2-15.4
	Cooling post M2	Wijbrans and McDougall [23]	K/Ar Hb	15.9
	Cooling post M2	Wijbrans and McDougall [23]	$^{40}Ar/^{39}Ar$ Hb	15.6-16.1
	Cooling post-M2	Andriessen [27]	Rb/Sr WR-Musc	15.3
	Post-M1 resetting + Mixing	Wijbrans and McDougall [26]	K/Ar WM	16.4
	Cooling post-M2	Andriessen *et al*. [22]	K/Ar Musc	10.2-15.2
	Cooling post-M2	Andriessen [27]	K/Ar Musc	13.4
	Mixing	Wijbrans and McDougall [23]	K/Ar Musc	12.8-16.3
	Cooling post-M2	Andriessen *et al*. [22]	K/Ar Bio	10.8-12.7
	Cooling post-M2	Andriessen [27]	K/Ar Bio	12.9
	Cooling post-M2	Andriessen [27]	Rb-Sr WR-Bio	12.4
	Cooling post-M2	Wijbrans and McDougall [23]	K/Ar Bio	10.1-10.6
VI	M1	Keay [24]	U/Pb zircons	40.7
	Migmatisation post M2	Keay *et al*. [29]	U/Pb zircons	16.8-20.7
	Magmatism post M2	Keay *et al*. [29]	U/Pb zircons	11.3-15.4
	Cooling post-M2	Wijbrans and McDougall [23]	K/Ar Hb	16
	Cooling post-M2	Wijbrans and McDougall [23]	$^{40}Ar/^{39}Ar$ Hb	15.0
	Cooling post-M2	Andriessen [27]	Rb/Sr WR-Musc	12.9-14.3
	Cooling post-M2	Andriessen *et al*. [22]	K/Ar Musc	11.4-12.1
	Cooling post-M2	Wijbrans and McDougall [26]	K/Ar WM	11.3
	Cooling post-M2	Andriessen [27]	K/Ar Musc	11.4-12.1
	Cooling post-M2	Wijbrans and McDougall [23]	K/Ar Musc	11.3-11.6
	Cooling post-M2	Wijbrans and McDougall [23]	$^{40}Ar/^{39}Ar$ Musc	11.8
	Cooling post-M2	Wijbrans and McDougall [26]	$^{40}Ar/^{39}Ar$ Musc	12
	Cooling post-M2	Andriessen [27]	K/Ar Phl	12.3
	Cooling post-M2	Andriessen [27]	Rb/Sr WR-Phl	12.7
	Cooling post-M2	Andriessen *et al*. [22]	K/Ar Bio	10.0-11.9
	Cooling post-M2	Wijbrans and McDougall [23]	K/Ar Bio	11.0-11.1
	Cooling post-M2	Wijbrans and McDougall [23]	$^{40}Ar/^{39}Ar$ Bio	11.4
	Cooling post-M2 perturbed by open system behaviour	Andriessen [27]	$^{40}Ar/^{39}Ar$ Bio	6.1
	Cooling post-M2 perturbed by open system behaviour	Andriessen [27]	K/Ar Bio	5.7-10.0
	Cooling post-M2 perturbed by open system behaviour	Andriessen [27]	Rb/Sr WR-Bio	5.7
	Weathering	Andriessen *et al*. [22]	K/Ar Bio	5.7

Abbreviations: **Amph** Undifferenciated amphiboles; **Bio** Biotite; **Chl** Chlorite; **Hb** Hornblende; **Musc** Muscovite; **Pg** Paragonite; **Phen** Phengite; **Phl** Phlogopite; **WM** Undifferenciated white micas; **WR** Whole-rock

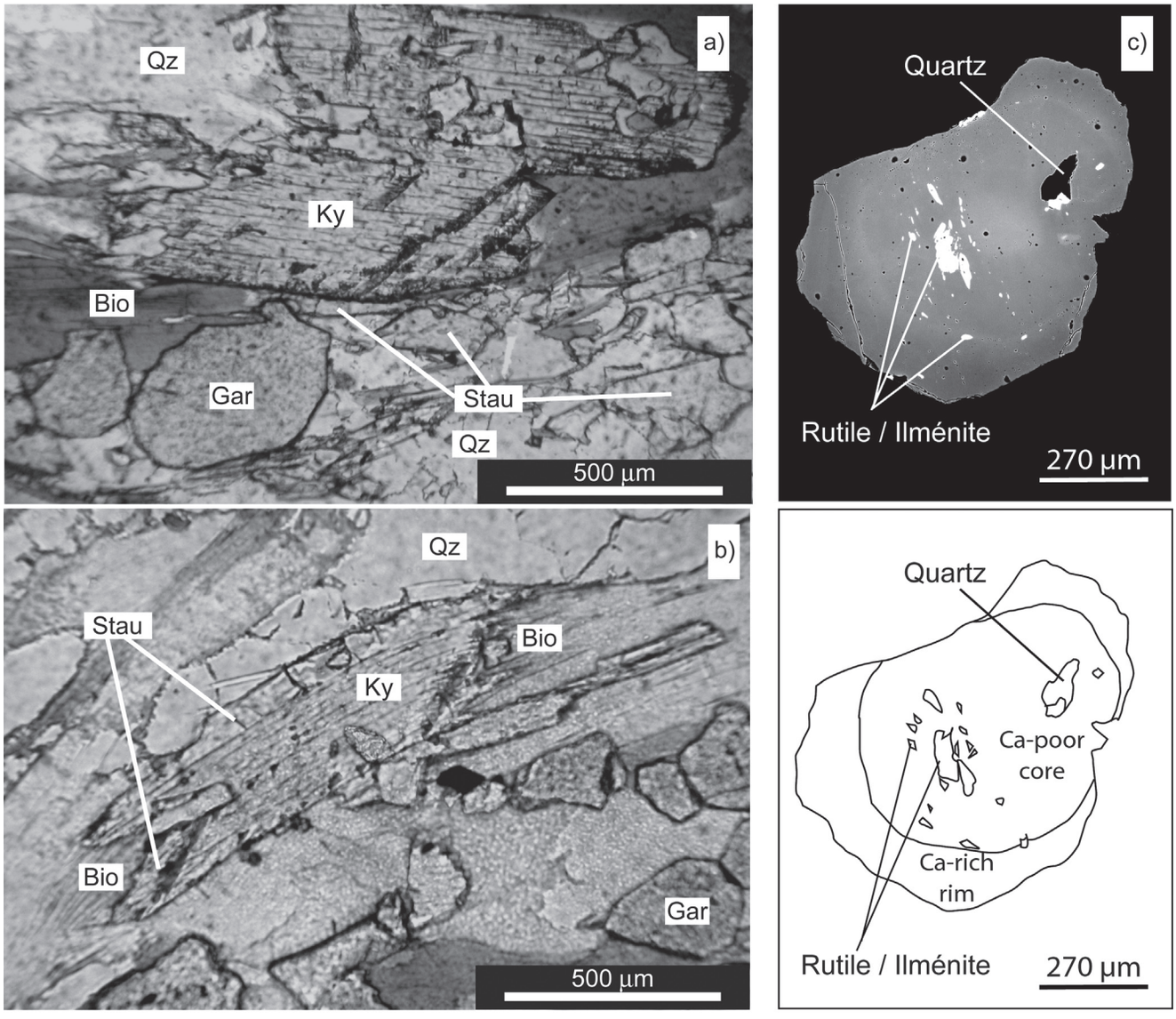

Figure 3: Sample NA 01 35, zone IV **a)** Photomicrographs showing the presence of late staurolite and biotite separating garnet and kyanite crystals. **b)** Photomicrographs showing staurolite and biotite growing at kyanite rims. **c)** SEM image of garnet zoning, revealing also the existence of rutile and ilmenite inclusions. An interpretation of the zoning pattern is suggested below, on the basis of electron microprobe analysis (Figure 5).

3.4. Sample NA 01 59, zone VI

Sample NA 01 59 is a migmatite, composed of ca. 50 % leucosome, 50 % melanosome. The leucosome consists of veins aligned with the foliation of the melanosome. The migmatite as a whole consists of quartz, biotite, garnet, plagioclase, sillimanite, K-Feldspar and muscovite (Fig. 2d). Garnets occur either as clusters in the leucosome fraction, or as inclusion-rich crystals in the melanosome. Sillimanite fibres appear as fringes around biotite aggregates in the melanosome. Plagioclase is albite rich (72-78 %). Biotite is rich in Al^{VI} (X_{Al}^{VI}=15 %) and Ti (X_{Ti}^{VI} =5 %) (Table III). Mg/(Mg+Fe) ratio ranges from 0.38 to 0.46 (0.42 in average). Individual biotite crystals present no zoning. Garnet is calcium and magnesium poor (X_{Ca}≈5 %, X_{Mg}≈10 %), and manganese and iron rich (X_{Mn}=15 %, X_{Fe}≈70 %). Zoning in garnet is characterized by antithetic Fe/Mn, or Mg/Mn evolution toward the rim (Fig. 5), over a distance of 50 to 100 μm. This type of zoning may be interpreted as a diffusion zoning driven by net-transfer reaction of garnet resorption [33].

4. Pressure and Temperature estimates

4.1. Methods

Temperature estimates may be performed on the basis of garnet/mica exchange thermometry. In low temperature samples, growth zoning is present in garnet. Equilibrium compositions are therefore expected from garnet rim/mica rim, and the temperature calculated from these compositions should correspond to the end of the crystallization process. In high temperature samples, growth zoning is absent. Temperatures obtained from rim composition would represent the temperature at which retrograde diffusive

Table III: Representative analysis of minerals

Mineral	Biotites												
Sample	NA 01 38, zone III				NA 01 35, zone IV			NA 01 27, zone V				NA 01 59, zone VI	
	(1)	(2)	(3)	(4)	(1)	(2)	(3)	(1)	(2)	(3)	(4)	(1)	(2)
Na_2O	0.00	0.14	0.00	0.02	0.20	0.00	0.22	0.32	0.32	0.37	0.09	0.14	0.34
MgO	8.57	8.67	8.46	9.02	7.16	7.40	7.59	13.03	8.29	8.63	9.74	7.89	8.16
Al_2O_3	17.83	16.92	17.32	17.22	19.65	19.14	19.48	18.60	19.19	19.47	20.07	18.96	19.39
SiO_2	36.58	37.57	38.34	35.76	36.08	35.68	36.24	36.47	35.42	36.05	36.79	35.89	35.62
K_2O	8.04	6.35	8.85	8.97	8.82	7.73	8.31	8.83	8.30	7.72	8.60	9.21	9.45
CaO	0.08	0.17	0.09	0.14	0.02	0.04	0.08	0.00	0.10	0.00	0.02	0.00	0.01
TiO_2	2.47	3.02	2.26	2.06	0.95	1.61	1.63	1.68	2.22	2.09	0.92	2.86	2.25
Cr_2O_3	0.01	0.00	0.00	0.04	0.00	0.00	0.01	0.02	0.00	0.07	0.00	0.06	0.00
MnO	0.42	0.44	0.51	0.29	0.21	0.12	0.00	0.08	0.11	0.12	0.23	0.07	0.27
FeO	17.57	17.12	18.16	18.29	19.31	18.73	18.49	14.29	17.11	17.00	16.56	19.87	19.96
Total	91.57	90.41	93.99	91.82	92.40	90.45	92.05	93.32	91.06	91.52	93.02	94.95	95.45
Si	2.845	2.920	2.916	2.811	2.812	2.817	2.813	2.752	2.772	2.789	2.799	2.740	2.715
Al^{IV}	1.155	1.080	1.084	1.189	1.188	1.183	1.187	1.248	1.228	1.211	1.201	1.260	1.285
Al^{VI}	0.477	0.467	0.466	0.403	0.614	0.594	0.592	0.403	0.539	0.561	0.596	0.443	0.454
Ti	0.144	0.176	0.129	0.121	0.056	0.095	0.095	0.095	0.130	0.121	0.052	0.164	0.129
Fe^{2+}	1.139	1.109	1.151	1.198	1.254	1.232	1.196	0.899	1.116	1.096	1.050	1.264	1.268
Mn	0.028	0.029	0.033	0.019	0.014	0.008	0.000	0.005	0.007	0.008	0.015	0.005	0.017
Mg	1.000	1.011	0.965	1.064	0.837	0.876	0.884	1.475	0.973	1.002	1.112	0.904	0.933
Ca	0.007	0.014	0.007	0.012	0.002	0.003	0.007	0.000	0.008	0.000	0.002	0.000	0.001
Cr	0.001	0.000	0.000	0.003	0.000	0.000	0.001	0.001	0.000	0.004	0.000	0.004	0.000
Na	0.000	0.021	0.000	0.002	0.030	0.000	0.033	0.047	0.048	0.055	0.013	0.021	0.050
K	0.798	0.630	0.859	0.900	0.878	0.779	0.823	0.851	0.829	0.762	0.835	0.898	0.920
Sum of the cations	7.593	7.456	7.610	7.722	7.685	7.589	7.631	7.776	7.653	7.610	7.674	7.702	7.772
Mg/(Fe+Mg)	0.468	0.477	0.4 56	0.470	0.400	0.416	0.425	0.621	0.466	0.477	0.514	0.417	0.424

Formulae calculated on the basis of 11 oxygens

exchange virtually ceased between garnet and micas. This would obviously lead to an underestimate of the metamorphic temperature associated with mineral crystallisation. Because of the high biotite/garnet volume ratio (more than 9/10 in these samples), biotite composition should not appreciably vary during retrograde exchange, so that using biotite/garnet core compositions should give a valuable approach of peak temperature. However, at temperatures above 600°C, core composition in garnet may also have been reset by diffusion and give a "closure temperature" rather than the crystallization temperature [34].

TWQ2.02 software with Ba96a and JUN92 data base [35, 36] has been used for most thermobarometric calculation and in particular garnet/biotite thermometry. Activity models consider non-ideal Ca-Fe-Mn-Mg mixing for garnet, and non ideal Mg-Fe-Ti-Al mixing for biotite. Garnet/phengite thermometry has been performed using the calibration of Green and Hellman [37]. The temperatures used to establish the PT path are discussed below. They have been reported in Table IV, and on Fig. 7.

4.2. Sample NA 01 38, zone III

As mentioned above, this sample contains an early high-pressure/low temperature assemblage that consists of phengitic white mica, plagioclase and garnet. The Si^{4+} content of white mica can be used to estimate a minimum pressure according to Massone and Schreyer [38]. It has been argued by Trotet *et al*. [39] that the Si^{4+} content may reflect the presence of pyrophyllitic substitution. When taking the analysis where the pyrophyllite content is the lowest and celadonite content the highest, the Si^{4+} content of phengitic white mica of 3.4 allows us to estimate a minimum pressure of 10 kbar at 500°C. Temperature for the high pressure assemblage can only be estimated on the basis of the phengite/garnet thermometer [37], although the experimental conditions do not fit the present Mg-rich composition of phengites (Mg/(Mg+Fe)=0.60 to 0.66) and pressure-temperature range. The temperatures obtained from phengite/garnet inclusions in the plagioclase are in the range 475-485°C. In sample NA 01 38, garnet grew in equilibrium with phengite and plagioclase, but garnet from the matrix is replaced by biotite at its rim. Rim-rim calculations have been taken into account for a garnet-biotite thermometry, assuming local equilibrium with biotite during the breakdown of garnet into biotite (Table IV). Temperatures fall in the range of 470-570°C. Note that the calculation of the local grossular-pyrope-anorthite-muscovite-phlogopite equilibrium with TWQ 2.02 and the Ba96 database gives an intersection at 5.5 kbar, 480°C which may correspond to the reaction producing biotite in the sample.

Table III (continue)

Mineral	White micas														
Sample	NA 01 38, zone III									NA 01 35, zone IV			NA 01 59, zone VI		
	(1)	(2)	(3)	(4)	(5)	(6)	(7)	(8)	(9)	(1)	(2)	(3)	(1)	(2)	(3)
Na_2O	0.13	0.14	0.15	0.17	0.13	0.41	0.15	0.21	0.25	1.07	1.25	1.29	0.63	0.48	0.63
MgO	2.20	2.98	2.63	2.47	3.01	1.06	3.07	1.36	0.97	1.09	0.63	0.67	0.89	0.73	0.79
Al_2O_3	28.39	27.65	26.99	27.40	26.83	32.62	28.47	32.78	32.52	34.62	35.17	35.80	34.68	34.94	34.91
SiO_2	52.43	51.03	49.93	49.50	50.34	48.22	52.11	47.10	45.25	47.44	46.55	45.68	45.24	45.69	45.33
K_2O	9.17	10.16	10.63	10.22	10.36	10.28	6.99	10.21	10.43	9.23	9.12	9.03	10.95	10.98	10.73
CaO	0.02	0.00	0.01	0.00	0.01	0.00	0.01	0.06	0.04	0.02	0.00	0.01	0.00	0.00	0.00
TiO_2	0.28	0.37	0.40	0.29	0.10	0.56	0.19	0.37	0.39	0.39	0.76	0.75	1.10	0.89	0.90
Cr_2O_3	0.00	0.00	0.00	0.05	0.00	0.03	0.02	0.00	0.03	0.00	0.00	0.00	0.07	0.00	0.00
MnO	0.15	0.12	0.11	0.16	0.11	0.02	0.00	0.10	0.08	0.03	0.00	0.00	0.03	0.05	0.06
FeO	2.68	2.89	3.11	3.41	2.80	2.73	2.78	2.88	2.97	1.26	1.12	1.06	1.52	1.57	1.54
Total	95.44	95.34	93.95	93.67	93.69	95.93	93.79	95.06	92.93	95.20	94.61	94.30	95.11	95.33	94.90
Si	3.453	3.402	3.398	3.377	3.421	3.201	3.447	3.161	3.122	3.140	3.099	3.053	3.041	3.059	3.048
Al^{IV}	0.547	0.598	0.602	0.623	0.579	0.799	0.553	0.839	0.878	0.860	0.901	0.947	0.959	0.941	0.952
Al^{VI}	1.653	1.570	1.558	1.577	1.566	1.748	1.662	1.749	1.761	1.835	1.854	1.868	1.783	1.811	1.809
Ti	0.014	0.018	0.020	0.015	0.005	0.028	0.009	0.019	0.020	0.019	0.038	0.038	0.055	0.045	0.045
Fe^{2+}	0.147	0.160	0.176	0.194	0.159	0.151	0.153	0.161	0.171	0.070	0.062	0.059	0.085	0.088	0.086
Mn	0.008	0.007	0.006	0.009	0.006	0.001	0.000	0.006	0.005	0.002	0.000	0.000	0.002	0.003	0.003
Mg	0.217	0.298	0.269	0.253	0.307	0.106	0.305	0.137	0.100	0.108	0.063	0.067	0.090	0.074	0.080
Ca	0.001	0.000	0.001	0.000	0.001	0.000	0.001	0.004	0.003	0.002	0.000	0.001	0.000	0.000	0.000
Cr	0.000	0.000	0.000	0.003	0.000	0.002	0.001	0.000	0.002	0.000	0.000	0.000	0.004	0.000	0.000
Na	0.017	0.018	0.019	0.023	0.017	0.053	0.019	0.028	0.033	0.137	0.162	0.167	0.081	0.062	0.082
K	0.771	0.865	0.923	0.890	0.899	0.871	0.590	0.875	0.919	0.780	0.775	0.771	0.940	0.938	0.921
Sum	6.827	6.937	6.973	6.963	6.959	6.959	6.740	6.978	7.013	6.952	6.954	6.970	7.041	7.021	7.027
of the cations															
Sum (K+Na)	0.788	0.883	0.943	0.912	0.916	0.924	0.609	0.903	0.952	0.917	0.937	0.938	1.021	1.001	1.003
Sum oct	2.017	2.029	2.003	2.023	2.032	2.005	2.120	2.047	2.032	2.013	1.979	1.994	1.959	1.973	1.975
Mg+Fe	0.364	0.458	0.445	0.446	0.466	0.257	0.458	0.298	0.271	0.178	0.125	0.126	0.175	0.162	0.166
Paragonite	0.023	0.026	0.028	0.030	0.020	0.063	0.023	0.036	0.042	0.144	0.175	0.180	0.096	0.076	0.095
Phlogopite	0.036	0.052	0.028	0.046	0.041	0.036	0.131	0.072	0.059	0.035	0.020	0.035	0.021	0.021	0.025
Pyrophyllite	0.199	0.101	0.040	0.071	0.078	0.054	0.383	0.080	0.029	0.068	0.035	0.034	0.000	0.000	0.000
Celadonite	0.264	0.313	0.371	0.317	0.348	0.163	0.069	0.094	0.106	0.083	0.085	0.040	0.130	0.115	0.108
Muscovite	0.477	0.508	0.532	0.534	0.514	0.683	0.393	0.718	0.763	0.669	0.684	0.710	0.753	0.788	0.772

Formulae calculated on the basis of 11 oxygens. End members decomposition made by matrix inversion (least square fitting of site occupancy)

4.3. Sample NA 01 35, zone IV

In this sample, because of the presence of growth zoning, only rim-rim calculations have been taken into account, assuming local equilibrium with biotite (Table IV). The presence of kyanite indicates a minimum pressure of 4 to 6 kbar at around 500-600°C. A pressure of 5 kbar is used in garnet/biotite thermometric calculations with TWQ. Temperatures are in the range 580-630°C. The temperature obtained for the staurolite-kyanite-almandine-quartz-water equilibrium is 600°C for P=5 kbar. Considering that staurolite is late in the assemblage, this appears to be a minimum temperature for the biotite / garnet / kyanite equilibrium. Moreover, the coexistence of staurolite and biotite places a minimum temperature of around 550°C. In summary, peak pressure and temperature conditions for this sample are taken as 580-630°C for a minimum pressure of 5 kbar.

4.4 Sample NA 01 27, zone V

In the absence of growth zoning and in the presence of retrograde exchange at garnet rims, the core composition of garnet has been used to calculate garnet/biotite equilibration temperature using the composition of neighbouring biotite (Table IV). The minimum pressure is estimated from the presence of kyanite. TWQ estimates for the temperature from garnet cores/biotite assemblages cluster around 700°C (675-750°C), which corresponds to a minimum pressure of 8.5 kbar for the presence of kyanite. Pressures of 7.5 to 8 kbars are also estimated from biotite/plagioclase/quartz/kyanite equilibria. A temperature of 750°C (highest temperature obtained from biotite/garnet thermometry) at such pressure is however unlikely since no partial melting occurs in the sample. On the basis of the location of the anhydrous dehydratation melting curve as reported in Le Breton and Thompson [40], we suggest that temperature did not exceed 700°C for a pressure of 8 kbar. The values obtained on the inclusions of biotite and plagioclase in garnet cores give low values of 600-620°C (TWQ) for pressures of 4.5 to 5.7 kbar, probably reflecting the retrograde exchange of Fe/Mg between the small biotite inclusions and garnet.

Table III (continue)

	Garnets													
Mineral *Sample*	NA 01 38, zone III					NA 01 35, zone IV			NA 01 27, zone V				NA 01 59, zone VI	
	(1)	(2)	(3)	(4)	(5)	(1)	(2)	(3)	(1)	(2)	(3)	(4)	(1)	(2)
Na_2O	0.00	0.16	0.00	0.01	0	0	0	0	0.07	0.09	0.12	0.02	0.01	0
MgO	1.01	1.24	0.88	1.47	0.96	2.03	2.02	2.09	4.32	3.61	3.38	4.21	2.29	2.67
Al_2O_3	21.16	21.38	21.29	20.71	21.36	21.13	21.38	21.48	21.17	21.3	21.64	21.26	21.15	21.09
SiO_2	37	37.75	37.41	36.98	37.44	37.9	37.82	37.67	36.91	38.14	38.55	37.72	36.6	37.35
K_2O	0	0.01	0	0.03	0	0	0.01	0.03	0.09	0	0	0.02	0	0
CaO	5.06	6.32	5.32	6.16	7.08	2.25	2.61	2.7	2.42	2.05	1.81	1.58	1.54	1.43
TiO_2	0.02	0.08	0.06	0.10	0	0.02	0.01	0	0.04	0.05	0.00	0.62	0	0
Cr_2O_3	0.00	0	0.03	0.03	0	0	0	0	0.02	0	0.00	0.04	0	0
MnO	4.94	4.12	8.49	3.35	4.71	2.03	2.23	2.78	3.47	3.99	4.49	4.73	6.93	5.82
FeO	31.26	29.76	28.54	30.35	29.09	33.17	33.36	32.77	32.26	30.87	31.03	31.29	31.42	31.61
Total	100.45	100.82	102.02	99.19	100.64	98.53	99.44	99.52	100.76	100.1	101.02	101.49	99.94	99.97
Si	2.989	3.011	2.983	3.005	2.999	3.074	3.048	3.035	2.947	3.036	3.042	2.977	2.974	3.014
Al	2.011	2.007	1.997	1.980	2.013	2.017	2.027	2.036	1.989	1.995	2.009	1.974	2.022	2.002
Ti	0.001	0.005	0.004	0.006	0.000	0.001	0.001	0.000	0.002	0.003	0.000	0.037	0.000	0.000
Fe^{2+}	2.105	1.978	1.896	2.056	1.942	2.242	2.240	2.200	2.147	2.048	2.041	2.058	2.128	2.126
Mn	0.337	0.278	0.572	0.230	0.319	0.139	0.152	0.189	0.234	0.268	0.299	0.315	0.476	0.397
Mg	0.122	0.148	0.105	0.179	0.115	0.247	0.244	0.253	0.517	0.431	0.400	0.498	0.279	0.323
Ca	0.438	0.540	0.455	0.536	0.608	0.196	0.225	0.233	0.207	0.175	0.153	0.134	0.134	0.124
Cr	0.000	0.000	0.002	0.002	0.000	0.000	0.000	0.000	0.002	0.000	0.000	0.002	0.000	0.000
Na	0.000	0.025	0.000	0.002	0.000	0.000	0.000	0.000	0.011	0.014	0.018	0.003	0.002	0.000
K	0.000	0.001	0.000	0.003	0.000	0.000	0.001	0.003	0.009	0.000	0.000	0.002	0.000	0.000
Sum	8.004	7.993	8.014	8.000	7.995	7.916	7.938	7.949	8.065	7.970	7.963	8.001	8.015	7.985
of the cations														
X_{Ca}	0.146	0.1834	0.150	0.179	0.204	0.069	0.079	0.081	0.067	0.060	0.053	0.044	0.044	0.042
X_{Fe}	0.701	0.6718	0.626	0.685	0.651	0.794	0.783	0.765	0.691	0.701	0.705	0.685	0.705	0.716
X_{Mg}	0.041	0.0504	0.035	0.060	0.039	0.087	0.085	0.088	0.167	0.148	0.138	0.166	0.093	0.109
X_{Mn}	0.112	0.0943	0.189	0.077	0.107	0.049	0.053	0.066	0.075	0.092	0.103	0.105	0.158	0.134
Mg/(Fe+Mg)	0.055	0.1834	0.053	0.080	0.056	0.099	0.098	0.103	0.194	0.174	0.164	0.195	0.116	0.132

Formulae calculated on the basis of 12 oxygens. Fe^{3+} content has been found to be negligeable from charge balance calculation.

4.5. Sample NA 01 59, zone VI

In the absence of growth zoning and in the presence of retrograde exchange at garnet rims, the core composition of garnet has been used to calculate garnet/biotite equilibration temperature using the composition of neighbouring biotite (Table IV). The biotite/garnet equilibrium and the stability of sillimanite allow the determination of a maximum pressure of 6 kbar for temperatures of 600-650°C. The sillimanite/plagioclase/garnet/biotite equilibrium corresponds to a pressure of ca. 4 kbar and a temperature of 628°C. Sample NA 01 59 lies structurally below sample NA 01 27, but records lower pressure and temperature. These two samples therefore do not belong to the same metamorphic gradient. The pressure-temperature conditions in the migmatic core record later stage during cooling and exhumation.

5. Geochronology

5.1. Methods

Rb/Sr isotopic analysis have been performed on whole-rock, white mica, biotite and garnet whenever it was possible in samples NA 01 38, NA 01 35, and NA 01 59 (Table V). Minerals were purified by heavy liquids and magnetic separation. Final handpicking under binocular microscope was realized in order to avoid inasmuch as possible mixed grains and inclusions. Rb and Sr have been separated by elution with HCl on Dowex AG50- X12 cation exchange resin and Ca has been eliminated from the Sr fraction by elution with ammonium citrate on the same resin. The measurement of the concentrations was done by isotope dilution on the same fraction as the isotopic composition. Strontium isotopic analysis was performed on Finnigan MAT 262 thermal-ionisation mass-spectrometer at CRPG. NBS 987 standard $^{87}Sr/^{86}Sr$ values were 0.710197 and 0.710229 at the date of the analysis. Rb concentration has been measured on ICPMS Elan 6000 at the SARM (CRPG). Standard $^{87}Rb/^{85}Rb$ value is 0.409 ± 0.01 (2σ) at the date of the analysis. Ages have been calculated with Isoplot [41].

5.2. Results

Sample NA 01 38 presents a well-defined isochron at 29.3±1.3(2σ) Ma (MSWD = 0.064) (Fig. 8). Whole-rock, white mica and garnet fall on the isochron. As shown before,

Table III (continue)

Mineral	Plagioclases									
Sample	NA 01 38, zone III		NA 01 27, zone V				NA 01 59, zone VI			
	(1)	(2)	(1)	(2)	(3)	(4)	(1)	(2)	(3)	(4)
Na2O	12.24	12.76	8.91	6.50	7.60	9.06	8.57	9.24	9.55	8.77
MgO	0.09	0.00	0.00	0.19	0.00	0.03	0.01	0.04	0.00	0.00
Al2O3	19.80	19.86	23.99	24.27	24.09	23.85	23.86	23.27	23.11	24.10
SiO2	70.73	69.76	62.43	62.95	63.41	61.00	61.09	62.90	63.88	61.38
K2O	0.12	0.10	0.10	0.09	0.12	0.08	0.36	0.52	0.48	0.25
CaO	0.12	0.04	5.03	5.41	5.19	5.62	5.58	4.38	4.18	5.24
TiO2	0.00	0.00	0.00	0.00	0.03	0.00	0.00	0.00	0.00	0.00
Cr2O3	0.00	0.00	0.00	0.01	0.00	0.01	0.00	0.00	0.00	0.00
MnO	0.08	0.00	0.00	0.07	0.00	0.15	0.01	0.00	0.00	0.00
FeO	0.23	0.00	0.21	0.09	0.10	0.35	0.00	0.00	0.00	0.06
Total	103.41	102.52	100.67	99.58	100.54	100.15	99.48	100.36	101.20	99.80
Si	2.996	2.984	2.753	2.778	2.780	2.720	2.733	2.782	2.799	2.734
Al	0.987	0.999	1.244	1.260	1.243	1.251	1.256	1.211	1.192	1.263
Ti	0.000	0.000	0.000	0.000	0.001	0.000	0.000	0.000	0.000	0.000
Fe	0.008	0.000	0.008	0.003	0.004	0.013	0.000	0.000	0.000	0.002
Mn	0.003	0.000	0.000	0.003	0.000	0.006	0.000	0.000	0.000	0.000
Mg	0.006	0.000	0.000	0.013	0.000	0.002	0.001	0.003	0.000	0.000
Ca	0.005	0.002	0.238	0.256	0.244	0.269	0.267	0.208	0.196	0.250
Na	1.004	1.056	0.760	0.555	0.645	0.782	0.742	0.790	0.810	0.756
K	0.006	0.005	0.005	0.005	0.007	0.005	0.021	0.029	0.027	0.014
K-Feldspar	0.006	0.005	0.005	0.006	0.008	0.004	0.020	0.028	0.026	0.014
Albite	0.988	0.993	0.758	0.680	0.720	0.741	0.720	0.769	0.784	0.741
Anorthite	0.005	0.002	0.237	0.313	0.272	0.255	0.259	0.202	0.190	0.245

Formulae calculated on the basis of 8 oxygens

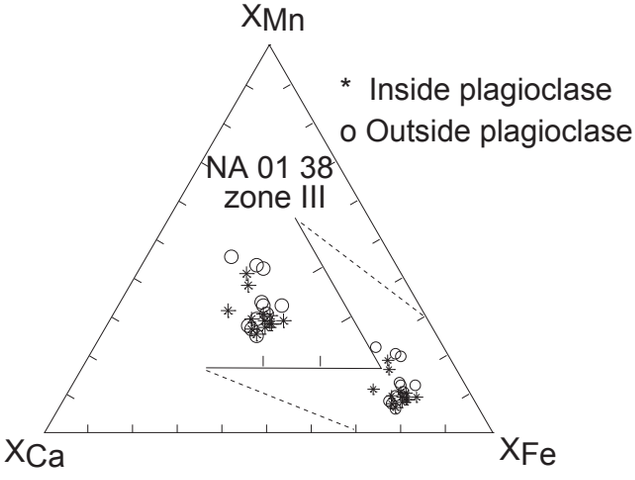

Figure 4: Garnet composition in sample NA 01 38. Comparison of the composition of garnets preserved inside plagioclase, and garnets enclosed in main foliation. Analyses correspond to both rim and core compositions of ca. 10 crystals

high-pressure white micas are dominant in this sample, belongs to the dominant garnet/phengite/plagioclase paragenesis, and are larger than 300 μm, whereas muscovite is late and small (<50μm). In order to select the phengite crystals for isotopic analysis, white micas have been handpicked from the 250-500 μm size - magnetic fraction. K/Ar ages of 28-29 Ma have been obtained in some white micas in the same zone by Andriessen *et al*. [22] and Wijbrans and McDougall [26]. Although obtained on phengite-rich mica separates, these ages have been interpreted by Wijbrans and Mc Dougall [26] as mixing ages of several generations of white micas. The 29.3 Ma age obtained on sample NA 01 38 can be explained by mixing of 37 % only of 45 Ma old high-pressure phengite and 63 % of 20 Ma old late muscovite, assuming a same $^{87}Rb/^{86}Sr$ ratio for both generations of micas. Taking into account that i) muscovite is less abundant than phengite in the sample and ii) mineral separation in the large size fraction favoured phengitic white micas, the hypothesis of mixing of two mica generations (M1 and M2-related) can therefore not explain the 29 Ma age. We can however assess the influence of mica mixing on the Rb/Sr ages. Assuming incomplete phengite/muscovite separation during the purification process and the residual presence of 30 % of 20 Ma old muscovite, the 29.3 Ma age could be considered as a mixing age between muscovite and a 33 Ma old phengite. This age is still lower than previous estimates for M1 metamorphism. We therefore suggest either that the Rb-Sr system was partially reset by diffusion after peak-pressure crystallization, or that phengitic white micas in sample NA 01 38 grew during the exhumation. For the high-pressure paragenesis, temperatures have been estimated at 475-485°C, which is lower than the closure temperature of the Rb/Sr system in white micas (ca. 500°C), so that the Rb/Sr age cannot be considered as a cooling age. However, phengite may have been partially open to Sr diffusion during

Table IV: Representative temperatures calculated by TWQ 2.02 [35]

Sample	*Comments*	*Mineral pair*		
		Garnet	*Biotite*	*T*°C
NA 01 38, zone III	Temperatures calculated for a pressure of 5kbars	(1) rim	(1) rim	484
		(2) rim	(2) rim	544
		(3) rim	(3) rim	468
		(4) rim	(4) rim	566
NA 01 35, zone IV	Temperatures calculated for a pressure of 5kbars	(1) rim	(1) rim	630
		(2) rim	(2) rim	619
		(3) rim	(3) rim	623
NA 01 27, zone V	Temperatures calculated for a pressure of 8.5kbars	(1) core	(1) inclusion	621
		(2) core	(2) rim	747
		(3) core	(3) rim	700
		(4) core	(4) rim	723
NA 01 59, zone VI	Temperatures calculated for a pressure of 6 kbars	(1) core	(1) rim	628
		(2) core	(2) rim	663

Numbers in parenthesis are reference numbers for the analysis given in Table II.

the exhumation since M2 metamorphic temperatures may have exceeds 500°C. The hypothesis of phengite crystallization below peak-pressure (during the exhumation) is supported by the fact that pressures estimated from ^{IV}Si content in phengites is ca. 10 kbar, whereas it has been demonstrated by Avigad (1998) that peak-pressure in the structurally higher zone I exceeds 12 kbars. Moreover, garnet plots on the isochron, and garnet/whole-rock age is 30 Ma, which suggests a garnet-phengite contemporaneous growth 30 Ma ago. This stage has been followed by the crystallization of late biotite at ca. 500°C, 6 kbar, at a date which may correspond to the 16-21 Ma M2 retrogression mentioned by Andriessen *et al*. [22], Wijbrans and McDougall [23], and Andriessen [27].

In sample NA 01 35, whole-rock, muscovite and biotite define an age of 5.2±0.7(2σ) Ma. As far as we know, this is the lowest age obtained by Rb/Sr, K/Ar, or ^{39}Ar/^{49}Ar from this zone. Such low Rb/Sr ages on biotite-whole-rock pairs have however been already described in gneisses from the migmatitic core [27]. Since the whole-rock Sr composition is dominated by muscovite (WR and muscovite are close to each other on the isochron), it cannot be demonstrated on this sample that biotite is in equilibrium with muscovite. Garnet falls well below this isochron, and corresponds to a low ^{87}Sr/^{86}Sr ratio. Alternatively, if an isotopic equilibrium between garnet and biotite is assumed, the age is 15.1±0.3 Ma. Garnet and muscovite define a meaningless age of 503±6 Ma. Because muscovite is in disequilibria with biotite as well as with garnet, we conclude that Sr isotopic ratio in the muscovite was acquired when whole-rock behaved as an open system. Garnet did not equilibrate at this stage, and retained the memory of the early Sr signature of the rock, prior to the bulk opening of the system. We cannot be sure if biotite was open or not with respect to Sr exchange at this stage. If not, the garnet/biotite age (15±0. Ma) could be meaningful and date the cooling of biotite below its closure temperature, assuming that the Sr isotopic ratio in garnet has been homogeneized during the amphibolite facies re-crystallization. The hypothesis of a fluid circulation accompanied by open-system behaviour at the rock scale has already been suggested by Andriessen [27]. In his sample Nax 78 (zone VI), the whole-rock biotite age is 5.7 Ma, the WR-muscovite age, which was interpreted as geologically meaningful, is 14.3 Ma, and the whole rock present-day ^{87}Sr/^{86}Sr ratio is very high (0.76043). Andriessen postulated that the initial Sr isotopic ratio with which biotite may have been equilibrated during late pervasive fluid circulation ("common Sr") was comprised between 0.711 and 0.715, and calculated an age of 6-7 Ma for this equilibrium. In this example, whole-rock and biotite are not in isotopic equilibrium, whereas whole-rock and muscovite are in equilibrium, which he explained by the fact that "mineral constituents have incorporated varying amounts of Sr from the circulating pore solution". The preservation of an isotopic ratio of 0.7126 in garnet from sample NA 01 35 is consistent with the hypothesis of open system behaviour, and indicates that the low Sr (ca. 0.710 for whole-rock) event took place before the muscovite re-equilibration stage.

Sample NA 01 59 is quite similar to sample NA 01 35. Whole-rock, biotite and muscovite define an isochron at 7.0±1.1(2σ) Ma. The initial Sr isotopic ratio is high (0.7334). Plagioclase has not been separated because it was optically difficult to distinguish plagioclase, K-feldspar and quartz, but since whole-rock plots to the left of both biotite and muscovite on the isochron and since plagioclase most probably dominates the Sr budget, it can be assumed from mass balance consistency that plagioclase plots on the isochron on the left with respect to whole-rock. Garnet plots below the isochron (^{87}Sr/^{86}Sr =0.724583), and is therefore out of equilibrium with the other minerals. Note that it was not possible to obtain a very clean garnet fraction because garnet was rare and inclusion rich, and therefore, the obtained garnet isotopic ratios most probably represent a mixing between pure garnet and whole-rock. Here again, the young age may represent open system behaviour of the Rb/Sr system postdating the crystallization of the migmatite. In this case, it can be concluded that both micas, and probably also plagioclase behaved as open system at that time.

5.3. Open system behaviour for Rb/Sr

Considering the three samples (Fig. 8) we may distinguish two groups of isotopic composition. One group is constituted by the whole-rock sample NA 01 38, and the garnets of samples NA 01 38, NA 01 35, and NA 01 59. This group is characterized by low present-day ^{87}Sr/^{86}Sr values (0.7186,0.7165,

Table V: Rb-Sr analysis of whole-rock and mineral separates of samples NA 01 38, NA 01 35, NA 01 59

Sample	*Mineral*	Rb (ppm)	Sr (ppm)	$^{87}Rb/^{86}Sr$	$^{87}Sr/^{86}Sr$ (2σ)	Ages (Ma)
NA 01 38	Whole Rock	135.64	74.85	5.06	0.718664 (32)	29.3±1.3 (2σ)
	White Mica	351.99	37.02	26.55	0.727607 (32)	(WR-WM-Gar)
	Garnet	0.18	3.28	0.15	0.716518 (357)	
NA 01 35	Whole Rock	143.47	118.66	3.38	0.736276 (26)	5.2±0.7 (2σ)
	Muscovite	181.65	206.56	4.76	0.736428 (32)	(WR-Musc-Bio)
	Biotite	510.38	8.59	165.81	0.748247 (27)	15.1±0.3 (2σ)
	Garnet	0.20	6.99	0.08	0.712652 (16)	(Gar-Bio)
NA 01 59	Whole Rock	143.19	55.91	7.15	0.733944 (18)	7.0±0.1 (2σ)
	Muscovite	201.67	27.82	20.24	0.735683 (230)	(WR-Bio-Musc)
	Biotite	534.22	2.46	605.98	0.793522 (32)	
	Garnet	10.315	2.12	13.57	0.724583 (106)	

Abbreviations: **WR** Whole rock; **WM** White micas; **Musc** Muscovite; **Gar** Garnet; **Bio** Biotite

0.7126, and 0.7246). Due to their low Rb/Sr ratio, garnets have essentially preserved their crystallization isotopic ratio. The whole-rock $^{87}Sr/^{86}Sr$ value for sample NA 01 38 recalculated at 5 Ma (whole-rock-biotite-muscovite age of sample NA 01 35) is 0.718292, and at 29Ma (whole-rock -muscovite-garnet age of sample NA 01 38) is 0.716580. It approaches in any case the Sr ratio preserved in garnets. The samples showing high Sr isotopic ratio are those in which the Sr content is low (45-120 ppm compared to 200-400 ppm in rocks with low Sr isotopic ratio [22, 27], this study), and $^{87}Rb/^{86}Sr$ is high (3 to 22 compared to 0.05 to 5 in rocks with low Sr isotopic ratio [22, 27], this study). First, we can suggest that $^{87}Sr/^{86}Sr$ ratios were reset by infiltration by a fluid with high Sr isotopic ratio (e.g. meteoric infiltration water) during late exhumation. Alternatively, we may postulate that the change in the whole-rock isotopic composition has accompanied metamorphic re-crystallizations of the metasediments under amphibolite-facies conditions. In this case, the garnet and the NA 01 38 WR isotopic compositions would be dominantly a remnant of the HP/LT conditions. This hypothesis is fully supported by petrology in sample NA 01 38, as explained above. Sample NA 01 35 presents growth zoning, with garnet cores characterized by the presence of rutile inclusions. Garnet cores may therefore appear as the remnant of the HP/LT paragenesis that has been predominantly replaced by MP/MT minerals in this rock.

6. Pressure-Temperature-time (PTt) paths

6.1. Construction of the PTt paths

The Pressure-Temperature paths have been drawn on Fig. 9 on the basis of the petrological results from this study. Moreover, it was further extended to the high-pressure stage as follows. The outermost part of the dome underwent blueschist facies conditions. Although there are no relics of HP/LT mineral assemblages for the inner, structurally lower part of the dome, we may expect that it underwent high-pressure/low temperature metamorphism as well. Peak-pressure depths for the four samples have been estimated from their respective structural positions, considering a current total thickness of 7 km (2 kbar) between zone I and VI, a pressure of 12 kbar in zone I [14], and a rock density of 2.7 kg dm^{-3}. Peak-pressures and depths increase accordingly from 12 kbar (44.4 km) in zone I, toward 13 kbar (48.1 km) in zone III, 13.45 kbar (49.8 km) in zone IV, 13.54 kbar (50.1 km) in zone V, and 13.9 kbar (51.5 km) in zone VI. The corresponding temperature was taken as 480°C for NA 01 38 in zone III (present study), which implies a high-pressure/low-temperature average geothermal gradient of 10°C km^{-1}. Along this gradient, the temperatures corresponding to peak-pressure conditions increase toward 498°C in zone IV, 501°C in zone V, and 520°C in zone VI. We assumed here that the structural thickness did not change significantly from the high-pressure/low-temperature metamorphism. This assumption will be discussed later.

Ages have been placed along the PT path according to the present Rb/Sr data and previously published data. We placed these ages into the PT path considering approximate closure temperature of ca. 500°C for K/Ar on hornblende, 350°C for K/Ar on muscovite, and 300°C for K/Ar and Rb/Sr on biotite.

An Eocene age of 45±5 Ma for HP/LT M1 metamorphism is considered for the intermediate structural levels of the dome as well as for deeper-seated samples [22-25].

For zone III (sample NA 01 38), we interpret the 29.3 Ma age obtained in the present study as that of phengitic white micas re-crystallization. This stage may represent a retrogressive evolution from the peak HP/LT stage (M1) testified in this zone by the presence of glaucophane [42]. The M2 re-crystallization is dated at 19.8-22.7 Ma by K/Ar, $^{40}Ar/^{39}Ar$, and Rb/Sr on muscovite. Rb/Sr and K/Ar ages obtained on biotite are indistinguishable and range from 12.5 to 14 Ma [23, 27]. NA 01 38 has been sampled close to sample 81-538 [23] which gives a K-Ar age at 12.5 Ma. We interpret the published K/Ar and Rb/Sr ages on biotite as cooling ages.

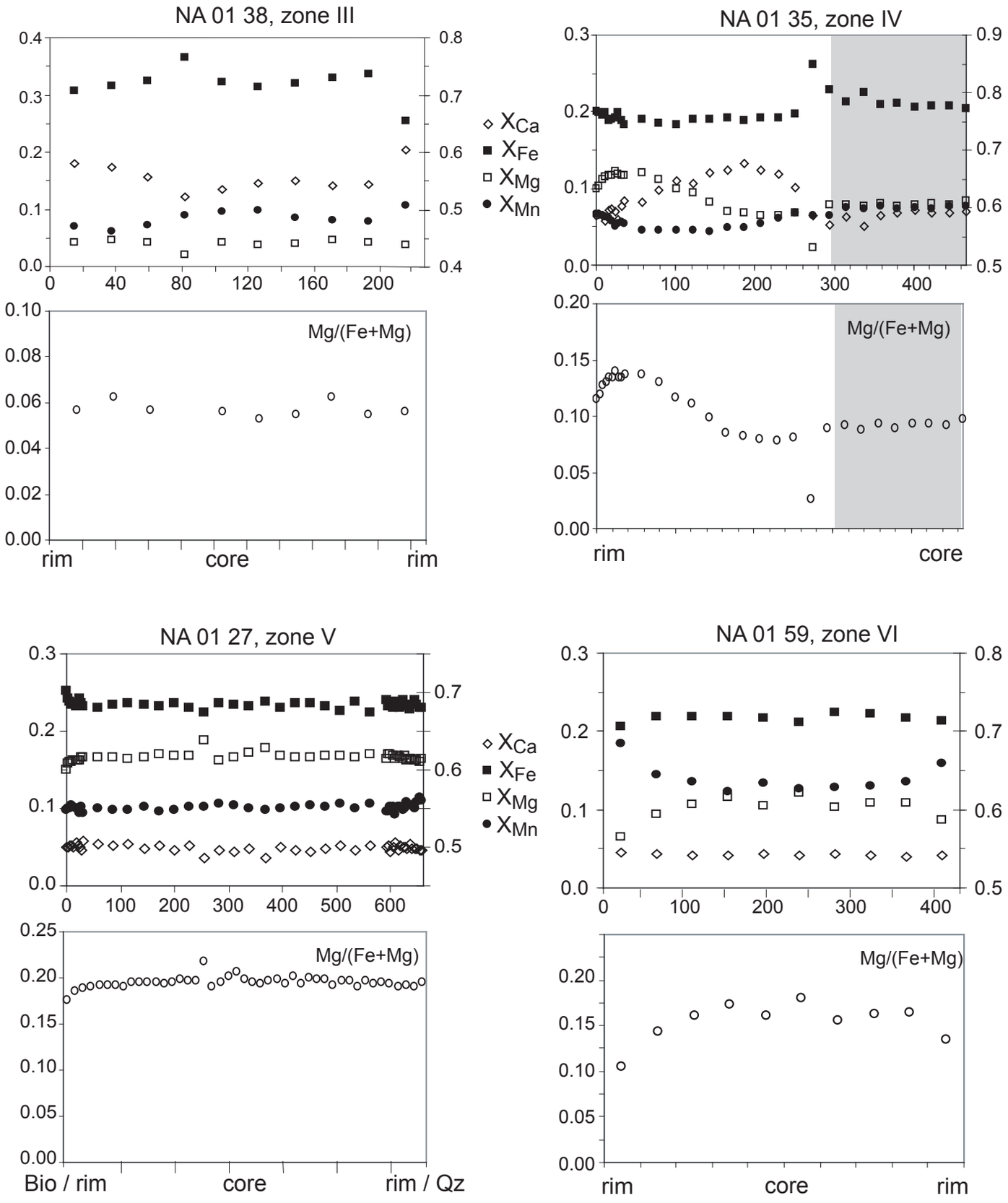

Figure 5: Garnet composition profiles. Ca, Mg, Mn on the left axis. Fe on the right axis. Distances in μm.

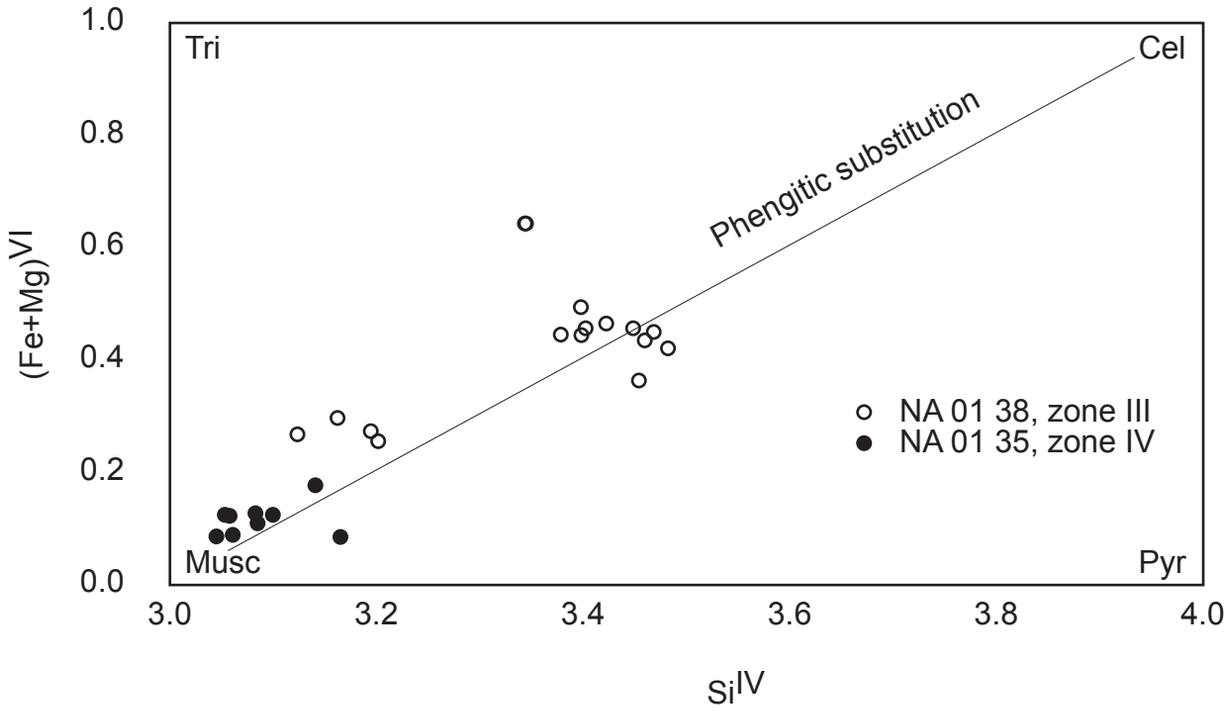

Figure 6: Composition of white micas. Abbreviations **Cel** Celadonite; **Musc** Muscovite; **Pyr** Pyrophyllite; **Tri** Trioctaedral white micas

In zone IV (sample NA 01 35), the oldest ages (15.2-17.9 Ma) are given by K/Ar and $^{40}Ar/^{39}Ar$ dating of hornblende [22, 23]. They are interpreted by these authors as cooling ages postdating M2 metamorphism. K/Ar ages on white micas are scattered from 10 to 16 Ma and may be mixing or cooling ages postdating M2. They cover the whole range between M2 ages and K/Ar data on biotite. K/Ar data on biotite range from 10.1 to 12.9 Ma in zone IV [22, 23, 27]. This range is restricted to 12.1 to 12.9 Ma if we consider only the area close to our own sampling point. These ages are equivalent to the K-Ar ages obtained on biotites from zone III and may represent cooling below the closure temperature of biotite. At last, the 5.2 Ma age obtained by Rb/Sr on biotite in this study is related to open system behaviour. Because 5-7 Ma ages obtained by K/Ar on biotite and $^{40}Ar/^{39}Ar$ on biotite have also been reported for zone VI [27], it is questionable if these ages have a geological meaning. If yes, they may correspond to a major fluid circulation that would have opened whole-rocks to Rb/Sr exchange.

In zone VI, the age of migmatization is constrained at 16.8-20.7 by U/Pb ages on zircons from the migmatite obtained by Keay *et al*. [29]. Some K/Ar ages on horblende indicate cooling below ~500°C between 15 and 18.8 Ma [22, 23]. K/Ar on muscovite (11.3-12.1 Ma [22, 23, 26, 27]) and Rb/Sr and K-Ar on biotite (10.0-12.7 Ma [22, 23, 27]), indicate further cooling below 300-350°C. As stated above, young Rb/Sr, K/Ar and $^{40}Ar/^{39}Ar$ ages on micas have been reported on samples from zone VI, which is consistent with our 7 Ma Rb/Sr age on sample NA 01 59.

6.2. Discussion of the PTt paths

The PTt paths reconstructed for samples from zones III to VI indicate the transition from a low to a high geothermal gradient. The metamorphic gradient is characterized by a general increase in maximum temperature recorded from zone III to V, in a MP/MT thermal regime (average gradient is ca. 25°C km-1) (Fig. 9). Exceptions are (i) blueschist relics in zone III, preserved thanks to limited temperature increase during the exhumation and (ii) lower P and T conditions in zone VI, which represent the position of this zone during crystallisation of the migmatites, after some exhumation and cooling following peak-temperature.

Considering that major re-crystallisations in MP/MT conditions are contemporaneous throughout the dome, samples which lies today at the same altitude underwent ca. 20 Myrs ago very different pressure and temperature conditions, thereby indicating that isotherms were not horizontal by that time and/or that the samples have been juxtaposed later by different amount of vertical displacement. Continuous cooling during exhumation is recorded successively by K/Ar and $^{40}Ar/^{39}Ar$ on hornblende (15-16.1 Ma), Rb/Sr, K/Ar and $^{40}Ar/^{39}Ar$ on muscovite (10.2-15.2 Ma) and finally on biotites (10.0-14 Ma). Cooling ages are similar for all samples from ca. 15 Ma, which implies no significant relative motion between them and that isotherms were subparallel to the topographic surface since then. Since on the other hand, medium-pressure/medium temperature metamorphic isograde underline the dome, dome forming is younger than 20 Ma. This brackets

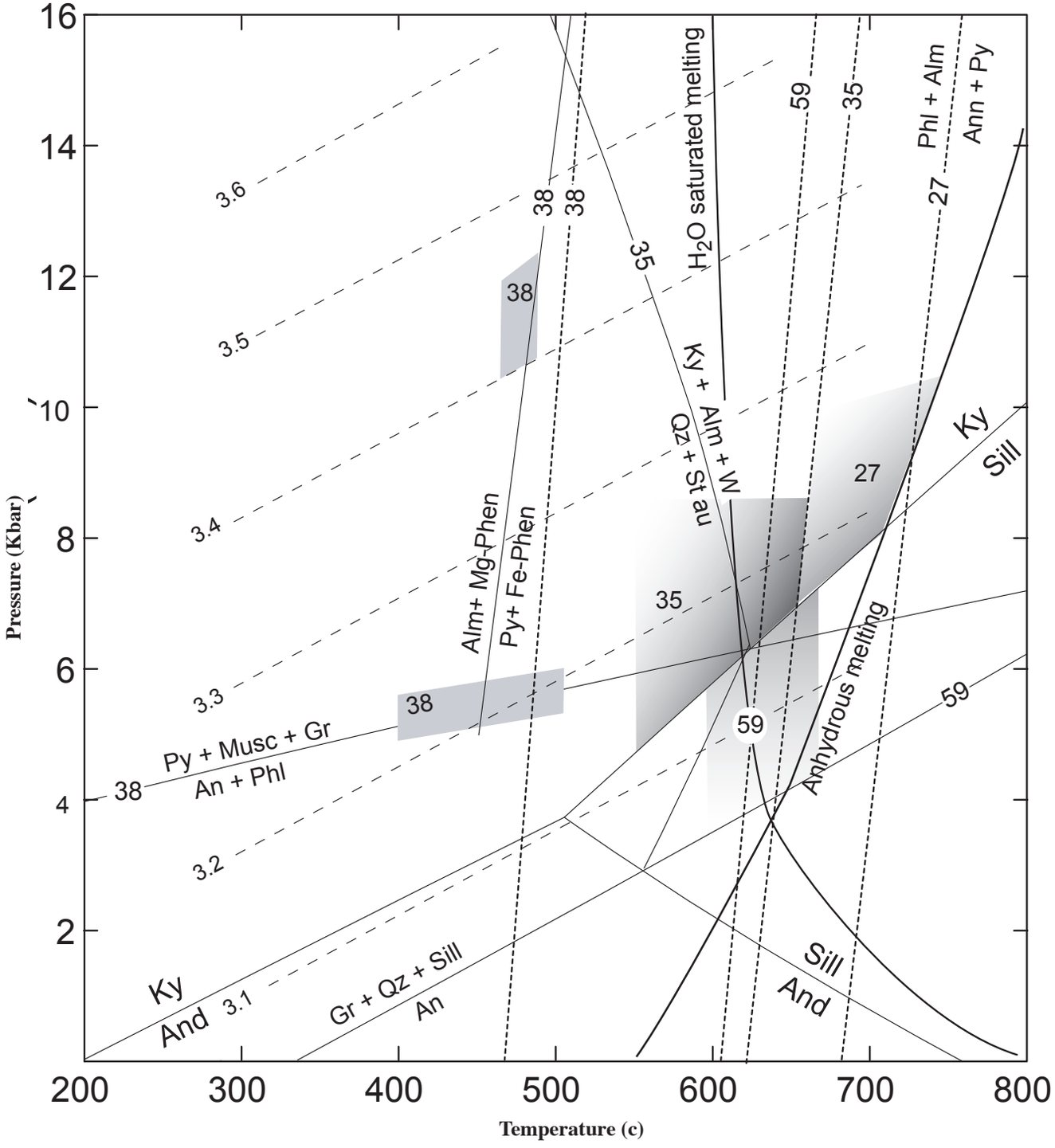

Figure 7: Pressure-Temperature paths of Naxos samples. Representative equilibria (including aluminosilicate triple point) are reported from TWQ 2.02 [35, 36]. Dashed lines: Si content of phengitic white micas are reported from Massone and Schreyer [38]. Anhydrous and water-saturated melting of metapelites as reported in Le Breton and Thompson [40]. Dotted lines: Biotite/Garnet equilibria from TWQ 2.02 [35, 36]. Boxes summarize pressure-temperature conditions for each sample as discussed in the text. ***Abbreviations***: **Alm** Almandine; **Py** Pyrope; **Gr** Grossular; **Phen** Phengite; **Musc** Muscovite; **Qz** Quartz; **Ky** Kyanite; **Sill** Sillimanite; **And** Andalusite; **Phl** Phlogopite; **Ann** Annite; **An** Anorthite; **Stau** Staurolite; **W** Water

dome formation between 15 and 20 Ma. This range differs from that estimated by Gautier *et al*. [9] (12-20 Ma), in that we considered Ar ages in hornblende in the external zones of the dome (zones I to III) as crystallization ages and did not considered them in the reasoning.

In the MP/MT gradient, the temperature difference between samples NA 01 38 (zone III) and NA 01 27 (zone V) exceeds 200°C. Considering that the structural thickness did not change

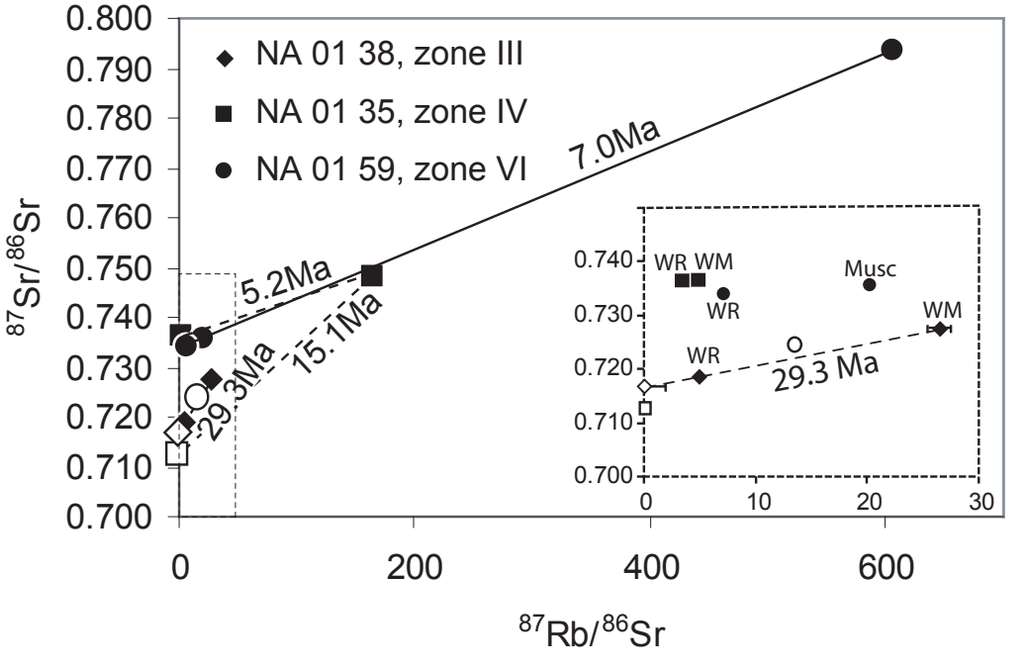

Figure 8: Isochron plot of Rb/Sr data. Open symbols: garnets.Filled symbols: whole rock, biotite and white micas not distinguished for simplicity in the main diagram. Inset is an enlarged view of the bottom-left corner.

over the metamorphic history, we have estimated above a temperature difference of 20°C only in the high-pressure/low-temperature gradient (Fig. 9). Sample NA 01 38 (zone III) did not undergo significant temperature increase during its exhumation, whereas the temperature increased by 200°C in sample NA 01 27 (zone V). The understanding of the differences in the exhumation histories from samples taken at different structural depths may help deciphering the thermal-tectonic evolution from high-pressure/low-temperature subduction setting to medium-pressure/medium-temperature back-arc setting. The Pressure-Temperature evolution during the exhumation of a crustal segment is controlled by i) the heat conduction in the crust expressed by the thermal diffusivity ii) the heat production by radioactive decay in the crust iii) the advection of heat possibly related to the exhumation or to a magmatic influx[2].

The composition of the crust (a gneissic basement, a pelitic and carbonaceous cover, and an ophiolitic sequence) was constant over the whole metamorphic complex in Naxos, as shown by the homogeneous nature of the conglomerates pebbles (ophiolitic remnants, marbles and schists), which collected the erosion products of the dome. The difference in the Pressure-Temperature paths between zones I and V can therefore not be explained by a difference in the thermal diffusivity and radioactive heat production characteristics. The difference between isothermal decompression in the outer part of the dome and decompression accompanied by heating in its central part may alternatively be explained by different advective fluxes. Differences in advective fluxes can result either from different exhumation rates (advection of the crust), or from different magmatic supplies (advection of material through the crust). In order to discuss the effect of varying exhumation rates, we have constructed the Pressure-Temperature paths for a simple one-dimensional model considering a semi-infinite advecting medium with surface temperature maintained to zero and undergoing upward motion [2, 43]. This solution can as a first approximation describe the thermal relaxation of the crust during exhumation, after subduction ceased to maintain low temperature condition at its base. The solution of the equation of heat transfer corresponding to these boundary conditions is given in Carslaw and Jäger p. 338 [44]. The results are shown for average crustal values of the radiogenic production (0.75 $\mu W/m^3$), the thermal diffusivity (10^{-6} m^2/s), and the heat capacity (2.25W/K) [2] (Fig. 9). Isothermal decompression is favoured by high exhumation rates compared to heat radiogenic production. Exhumation rates calculated in order to fit the maximum temperatures obtained during the exhumation decrease from 10 mm yr^{-1} for sample NA 01 38 in zone III, toward 1.8 mm.yr^{-1} in sample NA 01 35 in zone IV, 0.9 mm yr^{-1} for sample NA 01 27 in zone V, and 0.6 mm yr^{-1} for sample NA 01 59 in zone VI. This conflicts with the observations since the differences in the calculated exhumation rates exceed one order of magnitude, whereas the ages estimated for both HP/LT (ca. 45 Ma) and MP/MT (ca. 20 Ma) metamorphic stages are nearly identical over the metamorphic core complex and correspond to ca. 1 mm yr^{-1}. If the rocks from the core of Naxos (zones IV to VI) underwent heating during the exhumation whereas rocks from the outer part (zones I to III) did follow isothermal path, then it must have been because of local heat influx through magma injection.

However, the hypothesis of a constant structural thickness over the exhumation history is questionable. The nearly isothermal path over zones I to III is attested by the preservation of high-pressure/low-temperature assemblages. However, no remnant of high-pressure/low-temperature metamorphism has been found in the deeper part of the dome, and heating during the exhumation from peak-pressure conditions is hypothetical. Making the hypothesis that the pressure-temperature paths were initially isothermal in zones IV (600°C) and V (700°C),

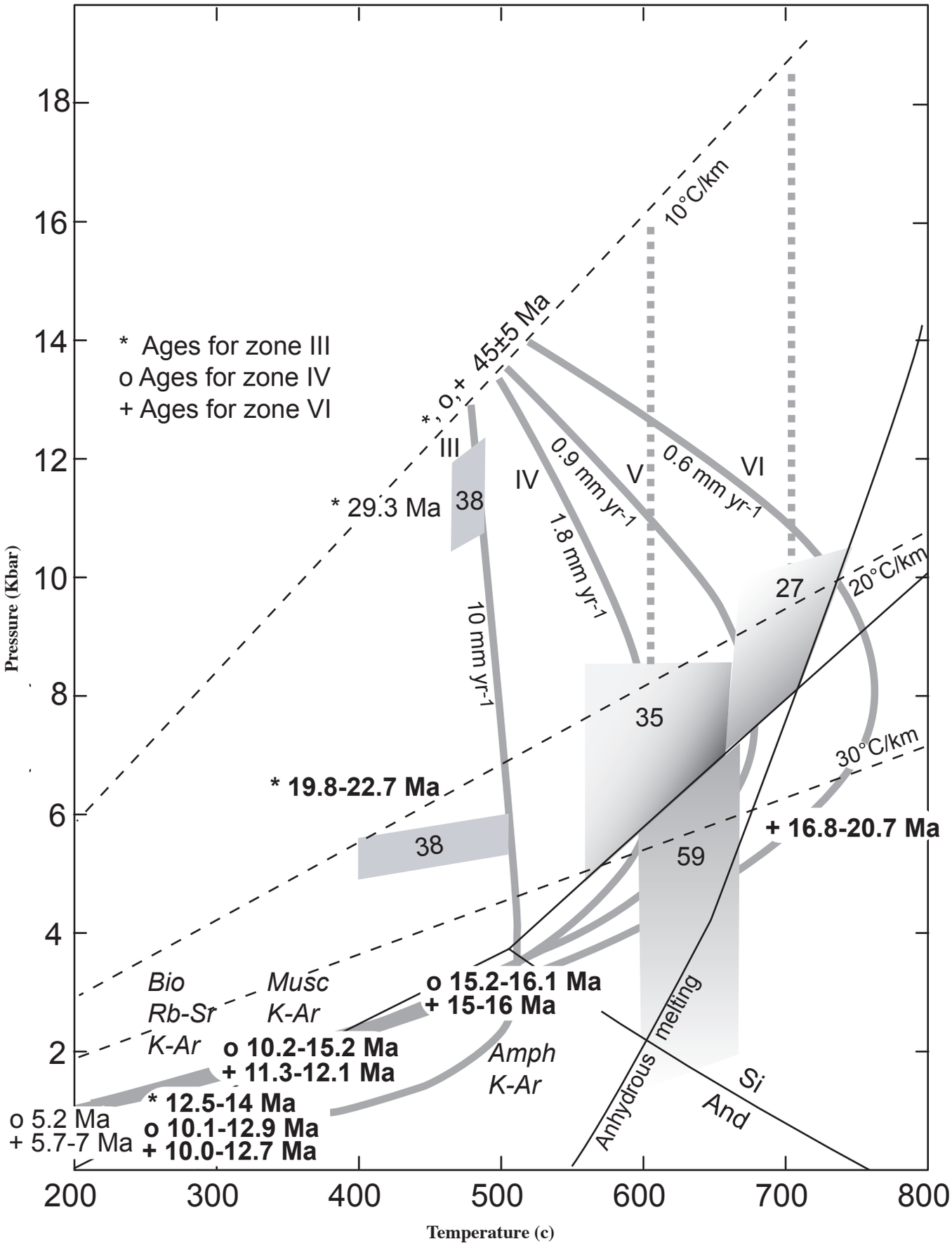

Figure 9: Pressure-Temperature-time paths of Naxos samples based on published geochronological data (indicated in bold on the figure, Table II) and on the present study (Tables III and IV). Approximate closure temperature have been taken as 500°C for K/Ar on amphibole, 350°C for K/Ar on muscovite, and 300°C for K/Ar and Rb/Sr on biotite. Average geothermal gradients are reported as dashed lines. Two possible sets of PT paths for the transition between LP/LT and MP/MT thermal regimes are considered. PT paths reported in solid lines correspond to the exhumation paths simulated i) considering that the four samples were aligned 45 Ma ago on the same HP/LT gradient (10° km-1) at depths increasing according to their present structural positions ii) considering the solution of the equation of heat transfer of an advecting medium according to Carslaw and Jäger (1959, p 338). Exhumation rates used in the calculations are indicated along the lines. PT paths reported in dotted lines correspond to the exhumation paths for the four samples assuming i) the exhumation paths were isothermal from HP/LT toward MP/MT conditions ii) the four samples were aligned on the same HP/LT gradient (10° km-1) 45 Ma ago.

the depths corresponding to the HP/LT gradient of 10°C/km are 60 km (ca. 16 kbars) and 70 km (ca. 19 kbars) respectively (Fig. 9). The initial (HP/LT) difference in depth prior to doming between zones III (50km, 13 kbars) and V (70 km, 19 kbars) would be of 20 km (ca. 6 kbars) whereas the present-day structural depth difference is 1.2 km (0.35 kbars). This converts to a very large value of homogeneous thinning (94 %). The same calculation performed between zones I and VI give a value for homogeneous thinning of 75 % at the scale of the crustal section exposed in Naxos. More probably, we can postulate that major displacement occurred between present day outer dome (I to III) and inner dome (zones IV to VI) and that these domains were put into contact during the exhumation between peak-PT conditions and MP/MT conditions.

7. Conclusions

1) Thermobarometry of three samples (NA 01 38, NA 01 35 and NA 01 27) taken on an east-west transect toward the centre of Naxos metamorphic dome record the increase in peak metamorphic temperatures from ca 500 to 700°C in the stability field of kyanite (above 5 to 8.5 kbar). These peak temperatures correspond to metamorphic re-crystallizations during the dominant MP/MT metamorphic context. Sample NA 01 38, in zone III, preserves an earlier metamorphic stage at a minimum pressure of 10 kbar and a temperature of 475-485°C, in a HP/LT environment. At the centre of the dome, the temperatures and pressures (650°C, in the stability field of sillimanite, i.e. below 6 kbar) recorded in the migmatites correspond to the later exhumation and cooling.

2) In zone III, a Rb/Sr age of 29.3+1.3(2σ) Ma is given by a garnet/muscovite/whole-rock isochron and is interpreted as the crystallization age of the phengite bearing metamorphic assemblage (at 480°C, 10 kbar).

3) The Rb/Sr data on the samples taken in the more internal parts of the dome give very low ages of 5.2 and 7.0 Ma. Such low ages have already been reported by different methods ($^{40}Ar/^{39}Ar$, K/Ar and Rb/Sr on biotite). Such samples systematically show very high whole-rock $^{87}Sr/^{86}Sr$ ratio (>0.730), which points toward open system behaviour. Garnet preserves the $^{87}Sr/^{86}Sr$ ratio prior to the opening of the system.

4) PTt path have been constructed in four points taken at different structural levels with help of published data. The PTt paths are characterized by i) an early metamorphic history in a high-pressure/low-temperature setting (average metamorphic gradient ≈10°C/km) 40-50 Ma ago and ii) a later metamorphic stage in medium-pressure/medium temperature setting (average metamorphic gradient 25°C/km). However, the initial depth and pressure for the deepest part of the dome is unknown. Making the hypothesis that the structural thickness was preserved during the HP/LT to MP/MT transition implies that the external part of the dome (zones I to III) followed near isothermal decompression whereas the inner part of the dome (zones IV to VI) was heated during M2 through magma injection. As an alternative, we suggest that the inner zones (IV to VI) also underwent near-isothermal decompression, which implies either a large general thinning during dome formation (75 %) or localized deformation that put into contact the inner and the outer part of the dome during rock exhumation.

The interpretation of the PTt path also suggests that the dome-shape structure on the west-east cross section has been acquired early in the cooling history (20-15 Ma), and that sample positions and isotherms have been horizontal since then.

Acknowledgments

This work has been supported by CNRS (IT program 2001 and "Coup de pouce à l'insertion des jeunes chercheurs" 2001) and UHP Nancy I (BQR 2000). Many thanks to Adonis Photiadis (IGME, Athens) who helped us with field work organization and has been our guide on the field. Sandrine Barda and Frédéric Diot of the Service d'Analyse in the UHP-Nancy are acknowledged for their help in electron microprobe analysis. Many thanks also to Béatrice Luais who offered much of her time to us during the development of Rb/Sr chemical separation in the new chemistry laboratory in Nancy. Laurie Reisberg gave us access to TIMS for Rb/Sr analyses, run by Catherine Zimmermann. Donna Whitney and two anonymous reviewers are acknowledged for their careful and constructive reviews.

References

[1] Dewey, J.F., Extensional collapse of orogens, Tectonics 7 (1988) 1123-1139.

[2] England, P.C. and Thompson, A.B., Pressure-Temperature-time path of regional metamorphism : I Heat transfert during the evolution of regions of thickened metamorphic rocks, J Petrol 25 (1984) 894-928.

[3] Vanderhaeghe, O. and Teyssier, C., Partial melting and flow of orogens, Tectonophysics 342 (2001) 451-472.

[4] Jansen, J.B.H. and Schuiling, R.D., Metamorphism on Naxos: petrology and geothermal gradients, Am J Sci 276 (1976) 1225-1253.

[5] Dürr, S., Altherr, R., Keller, J., Okrusch, M., and Seidel, E., The median Aegean crystalline belt: stratigraphy, structure, metamorphism, magmatism, in: H. Closs, *et al*. (Eds.), Mediterranean orogens: Alps, Appenines, Hellenides, Schweitzerbart, Stuttgart, 1978, pp. 455-477.

[6] Katzir, Y., Avigad, D., Matthews, A., Garfunkel, Z., and Evans, B.W., Origin and metamorphism of ultrabasic rocks associated with a subducted continental margin, Naxos (Cyclades, Greece), J Metamorphic Geol. 17 (1999) 301-318.

[7] Pe-Piper, G., Origin of S-type granite coeval with I-type granites in the Hellenic subduction system, Miocene of Naxos, Greece, European J Mineral 12 (2000) 859-875.

[8] Avigad, D. and Garfunkel, Z., Uplift and exhumation of high-pressure metamorphic rocks: the example of the Cycladic blueschist belt (Aegean Sea), Tectonophysics 188 (1991) 357-372.

[9] Gautier, P., Brun, J.-P., and Jolivet, L., Structure and kinematics of upper Cenozoic extensional detachment on Naxos and Paros (Cyclades Islands, Greece), Tectonics 12 (5)(1993) 1180-1194.

[10] Angelier, J., Essai sur la néotectonique et les derniers stades tarditectoniques de l'arc égéen et de l'Egée méridionale, Bull Soc Géol France 3 (XIX, n°3)(1977) 651-662.

[11] Angelier, J., Lybéris, N., Le Pichon, X., Barrier, E., and Huchon, P., The tectonic development of the hellenic arc and the sea of Crete: a synthesis, Tectonophysics 86 (1982) 159-196.

[12] Jolivet, L., Daniel, J.M., Truffert, C., and Goffé, B., Exhumation of deep crustal metamorphic rocks and crustal extension in arc and back-arc regions, Lithos 33 (1994) 3-30.

[13] Buick, I.S. and Holland, T.J.B., The P-T-t path associated with crustal extension, Naxos, Cyclades, Greece, in: J.S. Daly, *et al.* (Eds.), Evolution of metamorphic belts, Geological Society Special Publication, 1989, pp. 365-369.

[14] Avigad, D., High-pressure metamorphism and cooling on SE Naxos (Cyclades, Greece), European J Mineral 10 (1998) 1309-1319.

[15] Feenstra, A., Metamorphism of bauxites on Naxos, Greece, PhD Thesis, RU Utrecht, Geologica Ultraiectina, 1985, pp. 206.

[16] Haas, H., Diaspore-corundum equilibrium determined by epitaxis of diapore on corundum, Am Mineral 57 (1972) 1375-1385.

[17] Winkler, H.G.F., Experimentelle Gesteinsmetamorphose I; Hydrothermale Metamorphose karbonatfreier Tone, Geochim Cosmochim Acta 13 (1957) 42-69.

[18] Richardson, S.W., Staurolite stability in part of the system Fe-Al-Si-O-H, J Petrol 9 (1968) 467-488.

[19] Hoschek, G., The stability of staurolite and chloritoid and their significance in metamorphism of pelitic rocks, Contrib Mineral Petrol 22 (1969) 208-232.

[20] Luth, W.C., Jahns, R.H., and Tuttle, O.F., The granite system at pressures of 4 to 10 kbar, J Geophys Res 69 (1964) 759-773.

[21] Putlitz, B., Valley, J., Matthews, A., and Katzir, Y., Oxygen isotope thermometry of quartz-Al_2SiO_5 veins in high-grade metamorphic rocks on Naxos island (Greece), Contrib Mineral Petrol 143 (2002) 350-359.

[22] Andriessen, P.A.M., Boelrijk, N.A.I.M., Hebeda, E.H., Priem, H.N.A., Verdurmen, E.A.T., and Verchure, R.H., Dating the events of metamorphism and granitic magmatism in the alpine orogen of Naxos (Cyclades, Greece), Contrib Mineral Petrol 69 (1979) 215-225.

[23] Wijbrans, J.R. and McDougall, I., Metamorphic evolution of the Attic Cycladic Metamorphic Belt on Naxos (Cyclades, Greece) utilizing $^{40}Ar/^{39}Ar$ age spectrum measurements, J Metamorphic Geol. 6 (1988) 571-594.

[24] Keay, S., The geological evolution of the Cyclades, Greece - Constraints from SHRIMP U-Pb geochronology, PhD Thesis, Research School of Earth Science, Australian National University, Camberra, 1998.

[25] Martin, L., Deloule, E., Duchêne, S., and Vanderhaeghe, O. Isotope geochemistry of zircon overgrowths: a record of metamorphic history in Naxos (Greece). EGS-AGU-EUG Joint meeting. 2003. Nice.

[26] Wijbrans, J.R. and McDougall, I., $^{40}Ar/^{39}Ar$ dating of white micas from an Alpine high-pressure metamorphic belt on Naxos (Greece): the resetting of the argon isotopic system, Contrib Mineral Petrol 93 (1986) 187-194.

[27] Andriessen, P.A.M., K-Ar and Rb-Sr age determinations on micas of impure marbles of Naxos, Greece: the influence of metamorphic fluids and lithology on the blocking temperature, Schweizerische Petrologie und Mineralogie Mitteilungen 71 (1991) 89-99.

[28] John, B.E. and Howard, K.A., Rapid extension recorded by cooling-age patterns and brittle deformation, Naxos, Greece, J Geophys Res 100 (B7)(1995) 9969-9979.

[29] Keay, S., Lister, G., and Buick, I., The timing of partial melting, Barrovian metamorphism and granite intrusion in the Naxos metamorphic core complex, Cyclades, Aegean Sea, Greece, Tectonophysics 342 (2001) 275-312.

[30] Hollister, L.S., Garnet zoning : an interpretation based on the Rayleigh fractionation model, Science 154 (1966) 1647-1651.

[31] Anderson, D.E. and Buckley, G.R., Zoning in garnet : diffusion models, Contrib Mineral Petrol 40 (1973) 87-104.

[32] Lasaga, A.C., Richardson, S.M., and Holland, H.D., The mathematics of cation diffusion and exchange between silicate minerals during retrograde metamorphism, in: S.K. Saxena, *et al*. (Eds.), Energetics of Geological Process, Springer Verlag, New York, 1977, pp. 353-388.

[33] Spear, F., Metamorphic Phase Equilibria and Pressure-Temperature-Time path, in: P.H. Ribbe (Eds.). Mineralogical Society of America Monograph. Washington: Mineralogical Society of America, 1993, 789 p.

[34] Duchene, S. and Albarède, F., Simulated garnet-clinopyroxene geothermometry of eclogites, Contrib Mineral Petrol 135 (1999) 75-91.

[35] Berman, R.G., Internally-consistent thermodynamic data for stoechiometric minerals in the system Na_2O-K_2O-CaO-MgO-FeO-Fe_2O_3-Al_2O_3-SiO_2-TiO_2-H_2O-CO_2, J Petrol 29 (1988) 633-645.

[36] Berman, R.G. and Aranovitch, L.Y., Optimized standard state and solution properties of minerals. I. Model calibration for olivine, orthopyroxene, cordierite, garnet, and ilmenite in the system FeO-MgO-CaO-Al_2O_3-SiO_2-TiO2-H_2O-CO_2, Contrib Mineral Petrol 126 (1996) 1-24.

[37] Green, T.H. and Hellman, P.L., Fe-Mg partitioning between coexisting garnet and phengite at high pressure, and comments on a garnet-phengite geothermometer, Lithos 15 (1982) 253-266.

[38] Massonne, H.-J. and Schreyer, W., Phengite geobarometry based on the limiting assemblage with K-feldspar, phlogopite and quartz, Contrib Mineral Petrol 96 (1987) 212-224.

[39] Trotet, F., Vidal, O., and Jolivet, L., Exhumation of Syros and Sifnos metamorphic rocks (Cyclades, Greece). New constrains on the P-T paths, European J Mineral 13 (2001) 901-920.

[40] Le Breton, N. and Thompson, A.B., Fluid-absent (dehydratation) melting of biotite in metapelites in the early stages of crustal anatexis, Contrib Mineral Petrol 99 (1988) 226-237.
[41] Ludwig, K.R., Isoplot/Ex A geochronological toolkit for Microsoft Excel, Berkeley Geochronology Center Special Publication N° 1a (1999) 1-49.
[42] Buick, I.S., The metamorphic and structural evolution of the Barrovian overprint, Naxos, Cyclades, Greece, PhD Thesis, University of Cambridge, 1988, pp. 235.
[43] Mercier, L., Lardeaux, J.M., and Davy, P., On the tectonic significance of retrograde P-T-t paths in eclogites of the French Massif Central, Tectonics 10, NO.1 (1991) 131-140.
[44] Carslaw, H.S. and Jaeger, J.C., Conduction of heat in solids, in: (Eds.). Oxford: Clarendon Press, 1959
[45] Jansen, J.B.H., Geological map of Greece, Island of Naxos. 1977, Institute for Geology and Mineral Ressources: Athens.
[46] Vanderhaeghe, O., Structural record of the Naxos dome formation, in: D.L. Whitney, *et al*. (Eds.), Gneiss Domes in Orogeny, Geological Society of America Special Paper, 2004.